Published in final edited form as:
Adv Opt Mater. 2020 June 04; 8(11): . doi:10.1002/adom.201902117.

Seeing the Unseen: The Role of Liquid Crystals in Gas-Sensing Technologies

Carina Esteves, **Efthymia Ramou**, **Ana Raquel Pina Porteira**, **Arménio Jorge Moura Barbosa**, **Ana Cecília Afonso Roque***
UCIBIO, Departamento de Química Faculdade de Ciências e Tecnologia Universidade Nova de Lisboa Caparica 2829-516, Portugal

Abstract

Fast, real-time detection of gases and volatile organic compounds (VOCs) is an emerging research field relevant to most aspects of modern society, from households to health facilities, industrial units, and military environments. Sensor features such as high sensitivity, selectivity, fast response, and low energy consumption are essential. Liquid crystal (LC)-based sensors fulfill these requirements due to their chemical diversity, inherent self-assembly potential, and reversible molecular order, resulting in tunable stimuliresponsive soft materials. Sensing platforms utilizing thermotropic uniaxial systems—nematic and smectic—that exploit not only interfacial phenomena, but also changes in the LC bulk, are demonstrated. Special focus is given to the different interaction mechanisms and tuned selectivity toward gas and VOC analytes. Furthermore, the different experimental methods used to transduce the presence of chemical analytes into macroscopic signals are discussed and detailed examples are provided. Future perspectives and trends in the field, in particular the opportunities for LC-based advanced materials in artificial olfaction, are also discussed.

Keywords

gas sensing; liquid crystals; self-assembly; soft functional materials; volatile organic compounds

1 Introduction

The first observation of liquid crystalline behavior has been attributed to Reinitzer,[1] an Austrian botanist of the Institute for Plant Physiology of the German University of Prague, who was studying melts of cholesteryl acetate and cholesteryl benzoate and discovered they exhibited “double melting points.” The research on these strange and fascinating materials

cecilia.roque@fct.unl.pt.

Conflict of Interest
The authors declare no conflict of interest.

Author Contributions
C.E. and E.R. contributed equally to this work. The manuscript was written through contributions of all authors. All authors have given approval to the final version of the manuscript.

Europe PMC Funders Author Manuscripts

has gathered such an impetus, that currently liquid crystal (LC) based technology has permeated almost every section of society, from large industrial units to individual homes and offices. In particular, LC phases are widely used in display systems, for example, in liquid crystal displays (LCDs).[2] Liquid crystals, further detailed in Section 2, combine order and fluidity, that is they flow like conventional liquids but also they exhibit significant orientational order and in some cases positional order. These features are considered fundamental requirements for self-organization and formation of hierarchical structures. Additionally, they respond rather easily to external stimuli, such as electrical and magnetic fields, mechanical shear, pressure, surface effects, light, temperature, and chemical analytes with a change in their configuration that can be traced using a variety of characterization techniques. Due to this responsive and dynamic nature, the exploitation of LCs covers a wide range of discipline fields and applications in line with the current technological and societal needs, such as flat panel displays,[3] adaptive lenses and filters,[4,5] energy,[6–8] photonics,[9,10] biomedicine,[11,12] and design and architecture.[13,14]

An emerging field of research is the development of LC-assisted sensing technologies, since LC-sensing materials can be tailored to respond to targeted biological and chemical species.[15–21] Regarding biosensors, the concept involves either the imaging of targeted species displayed at solid surfaces, or sensing at LC/aqueous interfaces (LC thin films or droplets). So far, LC-based biosensors have been reported to detect a wide range of biomolecules such as glucose,[22] cholesterol,[23] lipids,[24] antimicrobial peptides,[25] proteins,[26,27] antigens,[28] pathogen DNA,[29] viruses,[30] bacteria,[31] or mammalian cells.[32,33] Nonetheless, the exploitation of LCs in biosensing devices has already been reviewed by other authors[16,19] and is outside the scope of this work.

The prime topic of this review is the development and application of LC-based soft systems in gas sensing, a field that has been gaining interest within the scientific community. Gas sensors represent an increasing market worth valued at USD 2.05 billion in 2018 (expecting to register a Compound Annual Growth Rate of 7.8% from 2019 to 2025[34]) and play a significant role in several fields such as industrial production (e.g., methane detection in mines[35]); automotive industry (e.g., detection of polluting gases from vehicles[36]); medical applications (e.g., clinical diagnostics[37]); indoor air quality supervision (e.g., detection of carbon monoxide[38]); environmental studies (e.g., greenhouse gas monitoring[39]).

Certain types of analytes can diffuse or even dissolve into liquid crystal materials and can change the LC order parameter, director orientation and/or phase properties. This leads to changes in their properties such as optical, electrical etc, which can be traced macroscopically. In this context, liquid crystalline materials can be implemented in gas-sensing platforms. When compared with the typical gas sensing materials such as semiconductor metal oxides[40] or conducting polymers that require high temperatures to operate,[41] LC-based sensing materials have been proven to exhibit higher selectivity (this term refers to sensor characteristics that determine whether it can respond selectively to a single or a group of analytes) even at low concentrations of analyte, in combination with the ability to operate at ambient conditions.[16] Furthermore, since this approach does not require the use of expensive and complex instrumentation,[42,43] LC-based sensing materials

are suitable for the development of portable,[44] low cost gas sensing devices for in situ, real time identification of gases and volatile organic compounds (VOCs).

In this work, we focus on the prevailing interaction mechanisms of LC sensing systems with gas analytes, implementing solely thermotropic systems. We report on the sensing capabilities of platforms that exploit not only interfacial phenomena,[45–47] but also changes in the bulk,[43,44,48] yielding various measurable outputs. Furthermore, we detail the strategies in which LCs amplify or directly participate in the molecular recognition of gases and VOCs and we provide details on the probing approaches and transduction (this term refers to the ability of converting variations in physical properties such as brightness or electrical conductivity into a measurable signal) methods employed so far. We elaborate on the tuned selectivity that can be achieved using LC gas sensors, thus further deepening our knowledge on molecular recognition processes. Overall, we intend to present a thorough and up to date review, which could serve as a central bibliographic source for both aspiring and experienced researchers.

First, we will introduce the most basic and fundamental aspects and properties of LCs. The remainder of the review is organized into the following categories. The first two sections are related with interaction mechanisms between LCs and VOCs, in systems where the LC is supported on a solid surface, either a chemically functionalized surface (Section 3.1) or a well-defined topography (Section 3.2). We continue with nematic systems doped with affinity molecules that can induce an orientation to the LC but can also interact with a specific gas analyte (Section 3.3). In Section 3.4, we present interface-systems that incorporate anchored or (bio)polymeric-encapsulated LC droplets. This is followed by Section 3.5 that discusses chiral nematic systems, which are either inherently chiral or most commonly the chirality is induced by a chiral agent.

At the end of each of these sections, the overall research conducted until now can be found in a tabulated format, containing all the necessary information regarding sensing materials, detected analytes, transduction methods and the LC system/gas interactions.

We then present in Section 4 the most crucial feature of LC-based sensing systems, which is the different experimental methods used to translate the presence of VOCs into macroscopic signals such as optical or electrical and provide detailed examples. Finally, we conclude with a discussion on future perspectives on the state of the field.

2 The Liquid Crystalline State

Liquid crystals are an intermediate state of matter between the crystalline and the conventional liquid states, displaying one or more phases (or mesophases), which arise from non-covalent and orientation dependent interactions between molecules of condensed phases.[49,50] LCs are to a certain degree, ordered fluids possessing orientational order and sometimes positional order. They also exhibit anisotropy in many of their physical properties that is a dependence on direction within the medium.

A key requirement for mesomorphism to occur is a highly anisotropic geometric molecular shape. For low molar mass LCs three main categories of LC molecules (or mesogens) can be

found: calamitic for rod shaped molecules (one molecular axis is much longer than the other two), discotic for disc-shaped molecules (one molecular axis is much shorter than the other two) and bent core or banana shaped (Figure 1).[51,52] A typical rod-shaped molecule is composed of two moieties: a relatively rigid core and a flexible chain. It is this elongated shape that allows the mesogens to align along their longer molecular axis. On the other hand, disk like molecules contain a flat aromatic core (usually based on benzene triphenylene or truxene) and flexible chains on the periphery. Due to this architecture, discotic molecules exhibit mesophases that involve the formation of stacks, creating higher ordered 2D columnar assemblies, such as rectangular, hexagonal, tetragonal, and herringbone (Figure 2). Finally, bent core mesogens can be described as V-shaped structures that incorporate a bent shaped rigid core, and their inherent polarity can lead to interesting and exotic mesophase formation such as polar smectic and biaxial nematic phases.[53–56]

In addition to low molar mass LCs, liquid crystal polymers and oligomers also exist. LC polymers consist of mesogenic groups (either rod-like, disk like or of more complex architecture) linked via flexible chains, called spacers.[57] Research interest can be traced back to the 1970s with the development of DuPont “Kevlar” poly(p-phenylene terephthalamide), a heat resistant and strong fiber as a replacement for steel and has many applications including aerospace engineering, military, mining and law enforcement protection or as an automotive component.[58] LC polymers are classified as main-chain, sidechain, combined main-chain/side-chain and cross-linked.

LC dimers, trimers, and oligomers in general were originally developed as “model compounds” for semiflexible main chain polymers[59] and they are comprised by two or more mesogenic units linked through a flexible spacer. They exhibit fascinating properties, which are quite different from the conventional low molar mass LCs. Their most striking feature is the dependence of their transitional behavior on the length and parity of the spacer (odd–even effect).[60] Currently, they have been attracting an increasing interest from researchers because they exhibit alternate novel mesophases.[61–63]

Depending on the thermodynamic parameter that determines phase formation, LCs are broadly classified as thermotropic or lyotropic. In thermotropic LCs, the building blocks are molecules and phase transitions occur by varying the temperature, e.g., by heating a solid or cooling an isotropic liquid. Lyotropic systems are mixtures of amphiphilic molecules and solvents mesophase formation is more concentration dependent (and less temperature dependent). Calamitic, discotic, and bent core systems are thermotropic LCs. Lyotropic mesophases form at specific concentrations of surfactant solutions.

In the following section, uniaxial nematic and smectic phases will be discussed in detail. These mesophases can be observed in both thermotropic and lyotropic systems, however we are interested in those formed by thermotropic compounds and mixtures.

2.1 Nematic, Chiral Nematic, and Smectic Mesophases

2.1.1 Nematic Phases—The simplest and most widely studied LC phase, comprised by achiral compounds, is the nematic phase (N). It is the least ordered mesophase, within which the molecules possess only orientational order of their long molecular axis and no positional

order of their center of mass. This preferred orientation is described by a unit vector called the director, $\hat{n}$ (Figure 2a). The director is an axis of full rotational symmetry where the states $\hat{n}$ and $-\hat{n}$ are equivalent, i.e., the N phase is apolar and uniaxial.

In reality, the LC molecules fluctuate around of the director, so the orientational order is far from perfect. In order to quantify the degree of molecular orientation relative to the director, the order parameter S is introduced and is defined as

$$S = \left\langle \frac{1}{2}\left(3\cos^2\theta - 1\right)\right\rangle \quad (1)$$

where θ is the angle between the director and the long molecular axis of each individual molecule and the brackets denote an average over all molecules. This expression can be also identified as the average of the second Legendre polynomial of cosβ, $P_2(\cos\beta)$. In an ideal and perfectly ordered nematic LC, $S = 1$, whereas in an isotropic fluid, $S = 0$. Like many LC properties, the order parameter is temperature dependent and decreases as the temperature reaches the isotropization point, also known as clearing point, indicating that increasing the temperature leads to a less ordered state. For a typical nematic material, the order parameter is in the order interval $0.5 \leq S \leq 0.7$. The order parameter S is often referred to as the nematic order parameter, however it is not restricted to the nematic phase. The expression in Equation 1 can be used to describe simply the degree of orientational order in uniaxial media.[64]

Finally, it should be noted that breaking one (or more) of the symmetries of the N phase (nonchirality, uniaxiality, a-polarity) can lead to a variety of more highly ordered nematic phases. such as i) the chiral nematic phase (discussed below), ii) biaxial nematic phases,[65,66] which are defined by two directors perpendicular to each other and have been identified experimentally in colloidal board-like systems,[67,68] a ternary lyotropic system that formed board-like micelles[69] and in thermotropic bananashaped systems,[70] iii) the nematic twist-bend[61,71–76] a chiral phase formed by achiral mesogens, characterized by a helical modulation of the orientational order with a pitch of the order of 10 nm.

2.1.2 Chiral Nematic (Cholesteric Phases)—By definition, a chiral object has a shape that cannot be superimposed on its mirror image. Chiral LC phases are usually formed by chiral molecules, that is molecules with a chiral center (it usually manifests by an asymmetry of molecular groups) or by doping a nematic host with a chiral substance.[77] The chiral analogue of the N phase is the chiral nematic phase (N* or cholesteric, Figure 2d). Within the mesophase, the chiral molecules organize in either a left-handed or right-handed helical arrangement, with the director twisting continuously around an axis (namely the helix axis), which is perpendicular to the director. The chiral nematic phase exhibits a reduced symmetry, when compared to the conventional nematic mesophase (N), due to the presence of chirality, however the condition $\hat{n} = -\hat{n}$ still persists. Additionally, similar to the N phase there is no positional order, only a localized orientational order, which can be described by Equation 1.

The distance needed for the director to rotate by an angle of 360° through the bulk is known as the pitch (P) and its magnitude is strongly dependent on temperature, but also flow and

externally applied fields. The pitch length can extend from a few hundred nanometers to infinity. If the pitch length is comparable to the wavelength of visible light, then selective reflection of visible light can occur due to the helical molecular arrangement. Factors such as the angle of incidence of the light, temperature and the pitch length of the helix can affect the color of the reflected light. The reflected light is circularly polarized and exhibits the same handedness as the helix, while circularly polarized light of opposite handedness is transmitted through the material.

2.1.3 Smectic Phases—Smectic LC phases are layered structures with a well-defined layer spacing or periodicity. They exhibit various degrees of orientational order (either orthogonal or tilted smectic phases), in-layer translational order (either liquid-like layers or layers with short range translational order) or both. Orthogonal are the phases where the director is perpendicular to the layers and the tilted smectic phases are characterized by an angle formed between the director and the layer normal. Usually, the molecules are still mobile and the layers can slide over one another. A result of the layering present is that smectic phases generally have higher viscosity and occur at lower temperature ranges than nematic phases.

The smectic A (SmA, Figure 2b) is an example of an orthogonal smectic phase, where furthermore the molecular centers of mass exhibit no long-range positional order within the layers. Since the director coincides with the layer normal, the directions $\hat{n}$ and $-\hat{n}$ are equivalent, hence the SmA phase is a uniaxial medium. The orientational order in the SmA phase is only slightly higher than in the N mesophase and can be quantitatively described by Equation 1. For smectic phases however it is useful to introduce a second order parameter namely the translational order parameter or simply the smectic order parameter. It is defined as

$$\sigma = \left\langle \frac{3\cos^2\theta_i - 1}{2} \cos\left(\frac{2\pi}{d} z_i\right) \right\rangle \quad (2)$$

where θ_i is the angle between the director and the long molecular axis of each individual molecule, z_i is the position of individual molecule's centers of mass if the z axis is chosen to coincide with the layer normal and d is the layer spacing. The brackets denote an average over all the molecules in the phase. The smectic order parameter σ is indicative of the macroscopic stability of the layers around the orientation direction.

An example of a tilted smectic mesophase is smectic C phase (SmC, Figure 2c) which is structurally similar to the SmA except that the molecules form an angle with the layer normal and the mesophase is biaxial. Finally, chiral smectic phases also exist, such as the SmC*, and they exhibit properties similar to N*. SmC* has a director that rotates as it progresses through the LC medium (Figure 2e). However, due to its layered nature there is also a tilt angle present. It is the precession of the tilt angle that results in a macroscopic helical structure. The helix can be unwound by surface forces giving rise to a surface-stabilized SmC*, which exhibits macroscopic polarization.[78]

In Figure 3, a few LC micrographs of samples prepared on untreated glass slides and viewed under crossed polarizers using a polarizing optical microscope (POM) are exhibited, illustrating the typical defects and textures that characterize the mesophases discussed above. Additionally, Figure 4 depicts typical mesogenic chemical structures exhibiting nematic, smectic, chiral and columnar mesophases.

2.2 Elasticity in Uniaxial Liquid Crystals

The ground state of the bulk N phase corresponds to a uniform spatial distribution of the director field. The presence of external stimuli, namely electric and magnetic field, shear and mechanical stress, or chemical analytes, can distort the director field, resulting in an elastic restoring force and increasing the free energy of the system. For an achiral nematic phase, in order to acquire an expression for the elastic contributions to the free energy the a-polarity of the phase ($\hat{n} = -\hat{n}$) and the fact that the medium is an incompressible liquid need to be considered. According to the theory developed by Oseen and Frank (see ref. [79]) and for the N phase, any deformation of the director filed can be expressed as a linear combination of three elementary elastic distortions, splay, twist and bend (depicted in Figure 5b). Therefore, the free elastic energy density of a bulk nematic consists of three terms, each one corresponding to contributions due to splay, twist and bend deformations respectively and is given by

$$F_d = \frac{1}{2}K_{11}(\nabla \cdot \hat{n})^2 + \frac{1}{2}K_{22}(\hat{n} \cdot \nabla \times \hat{n})^2 + \frac{1}{2}K_{33}(\hat{n} \times \nabla \times \hat{n})^2 \quad (3)$$

where K_{11}, K_{22}, and K_{33}, are the Frank elastic constants, each representing the resistance of the material to the splay, twist, and bend deformations respectively. Typically, the constants have the dimension of dynes with values ranging from 10^{-7}–10^{-6} and for nematics $k_{33} > k_{11} > k_{22}$. A fourth term should be added to Equation 3 when the nematic is in contact with a curved geometry (as in droplets, pores, cylinders), which is considered the surface interaction contribution and is named the saddle-splay term

$$-\frac{1}{2}K_{24}\nabla \cdot [\hat{n}\nabla \cdot \hat{n} + \hat{n} \times \nabla \times \hat{n}] \quad (4)$$

When the boundaries of the system are flat this term vanishes completely, however in curved geometries is important because it decreases the free energy of the system, whereas each other term increases it, if $K_{24} > 0$ which is the case for most materials studied so far regarding saddle-splay deformations. An insightful interpretation about the role of K_{24} can be found in the work of Selinger.[80] Knowledge of the elastic constants' values is of major practical significance, since they are related to any stimuli-based LC device.

Even though the expression for the free elastic energy density in Equation 4 has been developed for nematics, it can be modified to describe other mesophases as well. However, the restrictions dictated by the symmetry of the phase under study need to be taken into consideration each time. For example, the ground state of the chiral nematic phase is characterized by an unperturbed helical pitch with a well-defined value, p_o. In order to

include the spontaneous twist of the director, the helical wave vector $q_o = 2\pi/P_o$ is introduced and the free elastic energy density is modified as follows

$$F_d^* = \frac{1}{2}K_{11}(\nabla \cdot \hat{n})^2 + \frac{1}{2}K_{22}(\hat{n} \cdot \nabla \times \hat{n} + q_o)^2 + \frac{1}{2}K_{33}(\hat{n} \times \nabla \times \hat{n})^2 \quad (5)$$

where q_o is positive for a right-handed and negative for a lefthanded twist.

In the SmA phase, the twist and bend deformations are prohibited because the smectic layer thickness needs to be kept constant, therefore only the splay deformation is allowed

$$F_d^{SmA} = \frac{1}{2}K_{11}(\nabla \cdot \hat{n})^2 \quad (6)$$

2.3 Optical Properties of Uniaxial Liquid Crystals

As already mentioned, LCs exhibit anisotropy in many of their physical properties, due to the highly anisometric geometric shape of their building blocks. Perhaps the most significant and well-known anisotropic property is their birefringence, which means that their index of refraction depends on the direction of light propagation. Uniaxial systems are characterized by two refractive indices, the ordinary, n_o, and the extraordinary, n_e. More specifically, upon entering the medium, plane polarized light splits into two orthogonal component rays, ordinary and extraordinary, each travelling with differing velocities, their corresponding polarization planes being orthogonal, and hence the waves get out of phase.

The ordinary refractive index is constant and independent of the propagation direction, whereas the extraordinary refractive index varies with the ray propagation angle. Details on the mathematical expression of the extraordinary refractive index will be given in Section 2.5. When the rays recombine, after exiting the birefringent material, the polarization state will change because of the phase difference (more details will be given below).

For a nonchiral uniaxial system, the director coincides with the optic axis and by using the subscripts $\perp$ and $\parallel$ for the directions perpendicular and parallel to the director it follows that $n_o = n_\perp$ and $n_e = n\parallel$. The birefringence (Δn) is defined as the difference $n_e - n_o$, which for uniaxial nematic and smectic LCs becomes $\Delta n = n_\parallel - n_\perp$. Most calamitic LCs have a positive Δn resulting in a delayed extraordinary ray versus the ordinary ray as it travels through the LC medium.

However, the case of the chiral nematic phase is more complicated, because the optic axis coincides with the helix axis. Therefore, the optical axis is perpendicular to the local director. Then $n_e = n_\perp$ and n_o is a function of both $n_\perp$ and $n_\parallel$ and depends on the relative magnitude of the wavelength with respect to the pitch. Finally, chiral nematics exhibit a negative Δn. For a deeper analysis on the case of chiral nematics optics we refer the reader to more specialized texts.[50,77]

Earlier we mentioned that the ordinary and extraordinary components of light entering a nematic system travel at different velocities through the material. When they emerge from

Europe PMC Funders Author Manuscripts

the sample they are out of phase. The phase difference, known as optical retardation, is given by

$$\delta = \frac{2\pi}{\lambda}(n_e - n_o)d \quad (7)$$

where λ is the wavelength of light in vacuum and d is the sample thickness. It is the interference of these two rays which gives rise to the beautiful colors observed in optical textures. Optical retardation is the reason why the polarization state changes after passing through the anisotropic medium. Upon incidence of linearly polarized light, if the retardation is 90° then circularly polarized light emerges. If the retardation is 180° then linearly polarized light is produced, but along a direction perpendicular to the original polarization direction.

2.4 Liquid Crystals in Different Geometries

All LC applications rely on control the director orientation at a surface or an interface. From a practical point of view, the role of carefully chosen a surface or interface is to impose a specific alignment, which can propagate over macroscopic distances within the material, but also to confine the LC in a designated geometry. In this section, we will discuss briefly three types of LC interfaces, which have been exploited in gas sensing applications. However, we will avoid providing detailed information regarding the preparation of those systems because they typically are case specific.

The first type of interfaces is formed between a LC and a flat surface, typically a solid surface. This format has been widely explored in electrooptical applications, where a LC sample is enclosed between two glass substrates, which have been previously treated in order to provide a preferred orientation. Treatment methods include mechanical rubbing of substrates coated with organic polymers, photoalignment (exposure of photoreactive alignment chemicals to polarized light), oblique evaporation (usually SiO)[81,82] and particularly in LC-assisted gas sensing formats chemical functionalization of the surface in order to give rise to a range of intermolecular interactions between the interface and the LC (more details on chemically functionalized interfaces will be discussed in Section 3).

The preferred orientation of the director near an interface, set by alignment, is termed easy axis and is defined by the zenithal (θ) and azimuthal (φ) angles counted from the z and x axes respectively as seen in Figure 5c. Typically, the imposed orientation is either planar (in plane to the surface, $\theta = \pi/2$ and uniform azimuthal direction) or homeotropic (perpendicularly to the surface, $\theta = 0$) (Figure 6a,b). It should be noted however that hybrid geometries also exist when the LC material is confined within two surfaces with differing alignments. This type of format can be encountered in LC-mediated gas sensing investigations, where typically the upper interface in contact with the LC material is formed by an aqueous phase (or air). More detailed analysis about this last format can be found within the works of Popov et al.[18] and Miller et al.[83]

The most important factor that governs director profiles is the balanced interaction between the surface anchoring and the bulk elastic energies to minimize the total free energy of the

system. The anchoring energy, which is related with the bounding interface, expresses how much energy is needed to deflect the director from the easy direction, to which it is anchored. It is defined by a parameter W. A common expression to account for this contribution to the surface free energy has been described by Rapini and Papoular[84]

$$F_s = -\frac{1}{2}W\int(\hat{n}\cdot\hat{e})^2 dS \quad (8)$$

where ê is a unit vector along the easy axis.

The second type of interfaces is generated by the confinement of LCs in spherical geometries[85] which are typically dispersed within a second immiscible medium. Details regarding the preparation of this format for LC gas sensing investigations will be discussed in Section 3.4. The director configuration within LC droplets is dictated by the balance of the interfacial and elastic contributions to the free energy and the droplet size. However, the geometry of the system cannot sustain a continuous strain of the LC (such as some combination of splay, bend and twist) as dictated by the anchoring conditions. Instead topological defects are formed which can stabilize (or destabilize) the director configuration. A deeper analysis in the concept of topological defects can be found within the work of Kurik and Lavrentovich.[86]

Regarding the determination of the director profile within a droplet, a starting point would be the anchoring conditions. In the case of nematic droplets, which are topologically simpler, planar anchoring conditions result in a so-called bipolar configuration creating two-point defects in diametrically opposed positions of the surface of the droplet (boojums). On the contrary, under homeotropic anchoring the director field assumes a radial configuration, exhibiting a central point defect at the core of the droplet named hedgehog (see Figure 6c,d for a schematic representation).

It should be mentioned that a variety of different director configurations in spherical geometry have been reported,[87] either stable or metastable and some of them can be regarded as “intermediates” between the radial and bipolar profiles. By changing the anchoring conditions a transition from a radial nematic into a bipolar nematic configuration and vice versa is possible as was demonstrated by Volovik et al.[88] Starting from a bipolar nematic droplet and by gradually changing the surface anchoring, a progressive transformation of the director field was observed. The boojums disappear, while a defect ring appears in a plane perpendicular to the boojum axis. Subsequently the ring shrinks into a point defect located at one of droplet poles and then migrates into the core when the anchoring becomes homeotropic. Detailed information about director profiles in droplets can be found for example in the works of Lopez-Leon and Fernandez-Nieves,[89] Urbanski et al.,[90] or Gupta et al.[91] Finally, we should comment that more complex configurations arise when using smectic[92] or chiral phases.[93]

The last type of interfaces presented in this section is generated by the confinement of LCs in narrow cylindrical geometries. LCs confined in polymer fibers can also be used in gas sensing platforms.[44,94] Cylindrical geometries exhibit a higher symmetry than droplets and their configurations can provide insight complimentary to the spherical format.

For nematic LCs confined in cylinders with homeotropic anchoring, the cylindrical counterpart of the radial droplet configuration is not observed. A configuration where a disclination line forms along the core of the cylinder and a radial director field within the equatorial cross-section is not energetically favorable (see Figure 6e).[85] Instead a so-called escaped structure is preferred, where the line defect is replaced with a series of point defects. This allows the director to “escape” into the third dimension as it approaches the point defect, i.e., moving from the periphery to center of the geometry, the director bends into the cylinder axis. The direction of inclination within the medium is arbitrary, however alternating upwards and downwards inclinations have been observed experimentally.[95] This configuration is termed escaped radial with point defects (see Figure 6f) and for strong homeotropic anchoring it can be sustained down to 0.05 μm pore radius.[90]

Ondris-Crawford et al.[96] studied nematic liquid crystals in cylindrical cavities treated to promote planar anchoring. They achieved this unusual configuration by treating with a polyimide (Du Pont) the inner walls of the cavities of polycarbonate Nuclepore membranes. With the use of nuclear magnetic resonance, they succeed in identifying three different configurations, among which the so-called planar bipolar (see Figure 6g). Within the cavity the director field assumed a circumferential arrangement. The equatorial cross section was similar to the bipolar configuration, which has been already mentioned. Two surface disclination lines were running along the symmetry axis of the cylinder, located at the poles of the cross-section profile. More details about the rich variety of configurations in cylindrical cavities, including those arising from chiral nematic and smectic phases, can be found within the work of Urbanski et al.[90]

2.5 Optical Investigations of Uniaxial Liquid Crystals in Flat and Curved Geometries

As already mentioned in the previous section, LCs are able to manipulate the polarization of light due to birefringence. In fact, they can convert the polarization of light into linear, elliptical and circular, but also, they can change the main oscillation direction or reverse the rotation handedness. This is the basis of most electrooptic devices using LCs, where the sample is placed between two crossed polarizers. Determination of the director configuration of LCs confined is specific geometries is crucial for any LC-based application and can be primarily achieved using optical microscopy (either polarizing, or bright field, or both) by observing the patterns generated through the interaction of light with the LC.

Starting from the case of a well-aligned uniaxial nematic or SmA phase in a flat geometry between two crossed polarizers (see Figure 5d), upon normal incidence of light, the intensity of the transmitted light is given by

$$I = I_{\mathrm{o}} \sin^2 2\varphi \sin^2 \frac{\delta}{2} \tag{9}$$

where I_{o} is the light intensity exiting the first polarizer, φ is the position of the sample with respect to the coordinate system of polarizers (see Figure 5d) and δ is the optical retardation (defined in Equation 7). For a plane wave travelling through an anisotropic medium where the optical axis is inclined, it will experience an extraordinary refractive index

$$n_e = \frac{n_{\parallel} n_{\perp}}{\sqrt{n_{\parallel}^2 \cos^2\theta + n_{\perp}^2 \sin^2\theta}} \quad (10)$$

where θ is the angle of the optic axis and the direction of light propagation. For a homeotropic alignment $\theta = 0°$ and with the use of Equations 7 and 10 it follows that $\delta = 0$. The transmitted intensity (Equation 9) will always be zero for normal incidence of light and upon POM observation the texture appears dark for any angle φ. Due to this reason the homeotropic nematic and SmA texture is also called pseudoisotropic. When the alignment is planar then $\theta = 90°$ which leads to $n_o = n_{\perp}$ and $n_e = n_{\parallel}$. In this case, the transmitted light intensity depends on $\sin^2 2\phi$. It is zero for $\varphi = 0°$ and $\varphi = 90°$ and exhibits a maximum value when $\varphi = 45°$. Thus, upon rotation of the sample the texture will appear black each time the optic axis is parallel to one of the polarizer directions.

The effect of curved geometries (either spherical or cylindrical) on the optical behavior is more complex. The terms homeotropic and planar anchoring in those geometries are “valid” in the sense of how the director is oriented with respect to the interface. However, across the sample the direction of the optic axis varies with respect to the light propagation, unlike the case of well aligned planar and homeotropic flat geometries. For a detailed analysis, we advise the reader to refer to more specialized texts.[97] In the remainder of this section, the optical textures of nematic radial and bipolar droplets will be discussed.

Observed under crossed polarizers, a radial nematic droplet exhibit a distinctive Maltese cross pattern with four extinction branches in regions where the optic axis coincides with the direction of one of the polarizers (see Figure 7). The radial director configuration exhibits a spherical symmetry, consequently upon rotation the optical texture remains unchanged. The single point defect located in the droplet core can be better observed using bright field microscopy. On the other hand, the bipolar configuration is not spherically symmetric, thus under rotation of the sample the optical texture changes with respect to the crossed polarizers (Figure 7). When the droplets are observed along or perpendicular to the boojum axis they exhibit a cross pattern, while at intermediate angles a variety of patterns exists with respect to the crossed polarizers.[87,98] Using bright field microscopy one can readily identify the surface defects.

3 Functional Liquid Crystal Materials

The potential of LCs for the detection of volatile gases was initially discovered in 1965, by Fergason et al.[99] They prepared thin films of cholesterol-based mixtures for the detection (10 ppm or less) of hydrochloric acid (HCl), hydrofluoric acid (HF), nitric acid (HNO_3), nitrogen dioxide (NO_2), hydrazine (N_2H_4), and dimethyl hydrazine ($C_2H_8N_2$). The films exhibited color changes upon exposure, identifiable with the naked eye and with the exception of HF and HCl, the gas analytes could be distinguished from each other. Novac et al.[100] and later Poziomek et al.[101] studied nematic, smectic, and chiral systems for the detection of a wide range of organic vapors (such as acetone, methanol, acetic acid, and dioxane). Changes in the optical properties of the films were the indicator for the presence of VOCs. They concluded that the effect of gas analytes was to lower the isotropic transition

Europe PMC Funders Author Manuscripts

temperature of the LC compounds under study, to the test temperature. They also found that the most sensitive sensor was MBBA (a butylaniline-based nematic LC) or its mixtures with other derivatives of butylaniline. Since then, especially over the last 10 years, an on-going effort is being conducted by many research groups to understand and explore the potential applicability of different LC-based systems (nematic, smectic, chiral, columnar phases) in the gas sensing field.[16,18,20,102,103]

Discotic LCs were the first systems considered for sensing applications due to their appealing characteristics.[104–106] The columnar organization promotes charge carrier mobility within the stacks, due to π–π interactions between the aromatic cores, but also due to phase segregation of the aromatic and aliphatic moieties of the mesogens. Upon interaction with gas molecules, a disruption on the surface of discotic LC films occurs, causing orientational and positional variations, leading to conductivity changes. However, this concept has been almost abandoned nowadays, since the developed applications employed a homeotropic configuration which is very sensitive to diffusion effects.

In a typical LC-based gas sensor, the LC system is supported on a solid surface and needs to be in contact with the atmosphere, to be further exposed to VOCs. Upon interaction with gas analytes, a molecular reorganization of the LC occurs leading either to a director reorientation or a phase transition. This molecular response is usually very fast, reversible, and can be traced macroscopically (e.g., via POM).

The mesogens can assume a variety of different geometries depending on the interfacial boundary conditions. Several factors can affect the adopted geometries, namely the chemical functionalities or topography at the micro and nanoscales of interface, but also, for the pure LC molecules, the presence or absence of chemical dopants (e.g., chiral additives or affinity molecules) or nanomaterials (e.g., carbon nanotubes, CNTs). As such, the chemical and physical interactions between gas molecules and LC-based systems become far more complex.

Additionally, several secondary factors play an equally important role to the interplay between VOCs and LCs, such as the roughness of the substrate, the chemical functionalities of the sensing material itself, the LC layer thickness, the transport efficiency of the analyte molecules to the LC/interface, and the adsorption–desorption kinetics at the LC-interface.[46,47]

3.1 Liquid Crystal Systems in Chemically Functionalized Solid Surfaces

In surface-based LC devices, that is sensors using thin LC films supported on a functionalized surface, a principal mechanism responsible for the change in the LC molecular ordering is the competition between the gas analyte and LC molecules for the same binding sites on the substrate. The binding and adsorption of specific gas analytes to the surface of a substrate can be due to the chemical functionalization of the substrate with specific chemical groups (Table 1) or to the surface topography (Table 2).

A typical example of chemically functionalized surfaces for gas sensing is the case of transition metal salts, possessing high electron affinity cations (e.g., copper,[107–116]

aluminum,[117–123]) and deposited on solid surfaces (Table 1). Cyanobiphenyl-based LC systems, such as 5CB, assume a homeotropic orientation on these surfaces due to coordination interactions between the nitrile group of 5CB and the cation of the metal salt (serving as a binding receptor). When an analyte with affinity toward the substrate[124] is introduced in this environment, it will interact and adsorb to the surface of the substrate. Subsequently, the adsorption will disrupt the coordination interactions between the LC and the functionalized substrate, triggering an orientational transition within the LC system (Figure 8a).

In Figure 8b, the case of an analyte bearing a phosphoryl group (dimethyl methyl phosphonate, DMMP) is depicted.[110] In this case, DMMP adsorbs on a copper perchlorate modified surface, inducing a reorientation of 5CB from homeotropic to planar alignment. It is worth mentioning that LC reorientation can be monitored by measuring the intensity of polarized light transmitted through the LC system.

Surface functionalization studies have extended to perchlorate salts of metal ions[125,126] such as, gallium,[102] lead,[127] or manganese.[128] Hunter and Abbott[129] have also explored the possibility of tuning the anion in perchlorate-salt decorated surfaces in order to manipulate the LC anchoring to the binding surface, and hence increase the selectivity and sensitivity of surface-induced LC transitions triggered by gas analytes.

It should be noted that the recent study by Szilvasi et al.,[45] combining both theoretical and experimental works, clarified the influence of anions of transition metal salts on adsorbateinduced orientational transitions in 5CB. They concluded that when using nitrate salts to functionalize a surface, nitrate ions weaken the binding of 5CB to transition metal cations (when compared to perchlorate salts), which can lead to faster response times to chemical analytes. The hypothesis was verified in the case of $La(NO_3)_3$, $Zn(NO_3)_2$, and $Co(NO_3)_2$ functionalized surfaces, where they observed a six times faster response to DMMP, when compared to the corresponding metal perchlorate salts.

Shah and Abbott[130] investigated a carboxylic acid functionalized gold surface that promotes a uniform azimuthal orientation of 5CB molecules. The authors showed that an in-plane (azimuthal) reorientation of 5CB on this surface can be triggered by the presence of *n*-hexylamine. In this example, an optical cell was assembled where 5CB was placed between two obliquely deposited gold surfaces functionalized with a self-assembled monolayer (SAM) of 11-mercaptoundecanoic acid (MUA). The interactions between the carboxylic acid groups of the SAM and the nitrile group of 5CB promote an alignment parallel to the direction of gold deposition.[131] After exposure to *n*-hexylamine vapor, these interactions were blocked leading to an in-plane reorientation of the LC molecules of 90°. The hydrogen bond between the acidic moiety on the functionalized surface and the nitrile group of 5CB have a weaker bond strength (10–40 kJ mol^{-1}),[132] when compared with the acid–basic interaction between the acidic surface and the alkylamine (>70 kJ mol^{-1}).[131] They also demonstrated that the response of 5CB to *n*-hexylamine is strongly affected by mass transport of the analyte to the surface and can be manipulated by engineering the areal density of carboxylic acid groups presented on the gold surface.

Finally, we should mention the work conducted by Nayani et al.[133] In this work, it was demonstrated that the response and sensitivity to gas analytes can be improved substantially by customizing the properties of the employed LC system. The authors synthesized a nitrile-based LC mixture that assumes a planar configuration at the LC/air interface, contrary to the propensity for a homeotropical arrangement exhibited by cyanobiphenyl LCs, yet it maintains its chemoresponsiveness upon deposition on a metal-cation functionalized surface (in this study, La^{3+} perchlorate). It was shown that this hybrid, elastically strained, director configuration allows for a faster response to DMMP gas exposure, when compared to the 5CB case.

3.2 Liquid Crystal Systems in Solid Surfaces with Defined Topography and Unconventional Geometries

For the fabrication of well-defined topographies at the nano or microscales, different coating layers have been explored, such as rubbed polyimide,[134–136] or gold-coated topographies[46] which typically promote a uniform planar orientation of the LC (Table 2). For example, Kieser et al.[135] explored analytes and LC interactions via surface plasmon resonance (SPR). For this purpose, they used a unidirectional rubbed polyimide layer on top of a silver coated glass prism (a metal coated glass prism is mandatory in SPR). This was followed by the deposition of a nematic LC mixture (PYP-606:PYP-701, 1:1) by spin-coating (roughly 3.6 μm thickness), which led to a uniform homogeneous planar orientation of the LC mixture. When the sensing material was exposed to organic vapors, a decrease of the order parameter was detected, measured via SPR, and a phase transition to the isotropic state was induced. This, phase transition is dependent not only on the analyte concentration, but also on its shape and structure. For example, methylcyclohexane can induce a phase transition at lower concentrations than *n*-heptane due to its larger molecular volume. In the case of toluene, a lower concentration is needed to induce a phase transition, possibly due to the stronger interaction of aromatic compounds with the LC mixture.

Regarding gold defined surfaces, Sen et al.[46] have developed a gas sensor for nitrogen dioxide detection using the nematic cyanobiphenyl-based mixture E7 deposited on gold-coated polymer micropillars. The micropillar geometry facilitates the formation of a strong and uniform LC film by capillary forces, whereas the gold coating provides specific sensing chemistry for the analyte adsorption. Nitrogen dioxide molecules were dispersed into the LC film and adsorbed at the gold–LC interface, binding on to the gold via O,O-nitrito chelate formation. This results in a reduced interfacial energy of the gold–LC interface. When the surface density of the adsorbed nitrogen dioxide molecules is higher than a threshold value, an orientational transition occurs in the LC from parallel to perpendicular alignment and under crossed polarizers the transmitted light intensity diminishes (Figure 9). They also demonstrated that by measuring the rate of change of the light intensity at different analyte concentration, one can quantitatively determine an unknown concentration.

Equally significant is the work of Bedolla Pantoja et al.[47] where they showed that toluene triggers an orientational transition in 5CB films supported on chemically patterned microwells (fabricated either from gold or polystyrene deposited on borosilicated glasses). This geometry introduces a strain to the anchored LC. Exposure to toluene vapors decreases

the anchoring strength of the LC, thus allowing the director field to relax into a strain-free, uniformly aligned homeotropic state. They also demonstrated that the higher surface roughness of the gold substrates (which would induce local disorder in the LC) may contribute to a lower relative anchoring energy when compared to polystyrene substrates.

A few unconventional geometries have been also explored such as the encapsulation of LCs in polymer fibers,[94] a format which can be suitable for a sensing platform due to the flexibility, porosity and large surface-area-to-volume-ratios of the fibers (Table 2). For example, Reyes et al.[44] developed an organic vapor sensor with nonwoven mats comprised of coaxially electrospun LC-functionalized micron-thick fibers. The fibers consisted of a core of 5CB surrounded by a poly(vinylpyrrolidone) (PVP) sheath. They designed different mats, containing several types of fibers: uniformly cylindrical or irregular beaded fibers, in uniform or random orientations. At room temperature, the fibers scatter light strongly and upon exposure to toluene a rapid reduction in their brightness, to a more transparent state, was detected even with the naked eye. In Figure 10, a sample of uniformly cylindrical fibers is shown, as observed under the POM before, during and after exposure. It was hypothesized that the analyte vapors can penetrate the polymer sheath and diffuse into 5CB, thus lowering its clearing temperature. Complete transparency was reported above 3% volume fraction of toluene. Removal of the analyte vapors allows the system to recover to its initial state.

Another interesting example was demonstrated by Ohzono et al.[137] They developed a system working at ambient temperature and pressure, to detect chiral vapors based on nematic LCs. The device employed an achiral nematic LC anchored in sinusoidal open microgrooves with a frustrated interfacial alignment and a polarized optical microscope to detect structural changes in the periodic microstructure assumed by the LC (Figure 11). Within each groove, the LC exhibits a topological line defect, or disclination line, which looks like a zigzag. This is caused by the frustrated anchoring conditions, which do not allow a continuous director orientation without singularities. When in contact with chiral vapors, the disclination line responds accordingly through structural changes, depending on the enantiomeric excess of the vapor.

3.3 Doped Nematic Liquid Crystal Systems

So far, the discussion has focused on pure LC systems, where the surface-driven LC transitions are triggered by the interaction of gas analyte molecules and chemical functionalities of the surface or by topography surface features. In this section, we will discuss examples of nematic systems doped with affinity molecules that can either enhance or induce an orientation to the LC,[111,112,117,138] or, more interestingly, interact with the gas analyte[139,140] (Table 3). The most prominent example of the latter case has been demonstrated by Ding and Yang[139] where a gas sensor for butylamine vapor detection was developed. Here, 5CB was doped with lauric aldehyde (different concentrations ranging from 0.01 to 4 wt%) and used to fill copper grids placed on a glass slide, generating two LC interfaces—LC/glass and LC/air (Figure 12). When exposed to butylamine vapor, a bright-to-dark optical response was observed due to an orientational transition of the LC, triggered by a reaction between lauric aldehyde and butylamine.

When lauric aldehyde concentration is below 0.1 wt%, LC orientation is planar at the LC/glass interface and gradually turns into homeotropic at the LC/air interface. Once butylamine gas molecules diffuse into the sensing material, the reaction with lauric aldehyde occurs forming a transient imine which adsorbs at the LC/glass interface, causing an orientational transition from planar to homeotropic. For lauric aldehyde concentrations higher than 1 wt%, the director orientation at the LC/glass interface is homeotropic, and at the LC/air interface gradually becomes planar. In this case, lauric aldehyde reacts with butylamine, and 5CB changes its orientation to homeotropic at the LC/air interface. The proposed gas sensor appears to be reusable and its reversibility is attributed to the hydrolysis of the imine in humid/wet environments.

Pal et al.[141] and more recently Szilvasi et al.[138] have studied mesogenic mixtures containing specific moieties and their performance in response to the volatile compound DMMP. Pal et al.[141] studied a series of mixtures of 5CB with 4-pentyl-3′,4′-dicyanobiphenyl (DCB), a non-LC benzonitrile-based molecule which contains two nitrile groups, with varying concentrations from 0.9 to 2 wt% in DCB. Their goal was to investigate the quality and strength of the ordering assumed by the LC mixtures on copper-decorated surfaces, with a low surface density of copper. They found that the mixture adopted a sufficiently strong homeotropic alignment, due to the presence of the two nitrile groups in the DCB molecule (as mentioned previously the anchoring is facilitated by metal ion–nitrile coordination interactions). However, the LC mixtures exhibited a slow response to the presence of DMMP vapors (roughly 180 s), when compared to pure 5CB (15 s). Szilvasi[138] has combined computational chemistry and organic synthesis studies, showing that the selective fluorination of 5CB molecules can reduce the binding strength of their nitrile group to metal salt decorated surfaces. This hypothesis was tested on a mixture of pure 5CB and an *ortho*-fluorine modified 5CB (named FCB, which does not exhibit LC behavior) deposited on a variety of different surfaces decorated with perchlorate salts of Fe^{3+}, Al^{3+}, Ga^{3+}, La^{3+} and Zn^{2+}. When the mixture was exposed to DMMP a decrease in the response rate was observed (Figure 13). They concluded that this was due to the binding strength of the FCB molecule to the metal cation, which is weaker than the pure 5CB, due to the presence of the electronegative fluorine that withdraws electron density from the phenyl group and its nitrile group.

3.4 Liquid Crystal Systems Using Nematic Droplet Configurations

LC droplets have also been considered as potential candidates for gas sensing applications[42,142–145] (Table 4). When compared with the solid surface-based sensing systems described in previous sections, interface-anchored or (bio)polymericencapsulated LC droplets exhibit a larger surface area, which can be advantageous in chemical sensors designed for higher sensitivity. When LCs assume a spherical geometry, the molecular mechanism of gas sensing (recognition of the target volatile) occurs through a competition between the analyte and either the surface of (droplet) deposition or any components of the droplet itself.

Hu and Jang[143] described a gas sensing system where the LC, 5CB, is dissolved in organic solvents and forms droplet structures when spread onto treated glass slides. Two different

droplet patterns were detected, exhibiting distinctive optical textures. The first type results from spreading an ethyl alcohol solution containing 5CB onto a piranha-treated surface. After solvent evaporation, droplet formation occurs due to the hydrophobic nature of 5CB versus the hydrophilic nature of the piranha-treated surface. The droplets exhibited a fan-shaped texture, resulting from a homeotropic orientation at the air/LC interface and a random director orientation at the piranhatreated glass (Figure 14a). Sensitivity of the sensing material to room humidity was evaluated by exposure to room conditions: an optical change from bright to dark gradually occurs within 4 h. The second type of droplet pattern is formed after spreading a solution of 5CB in heptane onto an octyltrichlorosilane (OTS)-treated glass slide. Due to the hydrophobic nature of both solvent and treated substrate, 5CB molecules within the droplet assume a homeotropic orientation, exhibiting a dark-cross droplet texture (Figure 14b). The LC system is not sensitive to humidity, possibly because water molecules were not easily absorbed onto the surface, due to the hydrophobicity of OTS-treated substrate. The sensing material was exposed to organic vapors, such as heptane and ethyl alcohol. When the exposure occurs, a quick change in the optical appearance of the droplets (as observed with POM) from bright to dark is detected. After the removal of the organic vapor, the LC droplets return to their initial bright state, exhibiting reversibility of the system (Figure 14c).

Semeano et al.,[142] Hussain et al.,[42] and recently, Esteves et al.[43] studied self-assembled LC droplets encapsulated in an ionic liquid interface and dispersed within a biopolymer matrix, overall forming a hybrid gel. The anchoring of 5CB molecules, which is preferentially homeotropic, is promoted by the ionic liquid. The absorption of various gas molecules from distinct chemical classes into the hybrid gel matrix results in LC disordering and isotropization (depending on the analyte), leading to bright-to-dark optical changes. In the case of hydrophobic non-polar gas molecules such as hexane, the reorganization of the LC is mainly due to interactions between gas and LC molecules. For polar and protic compounds such as ethanol, an increased fluidity of the matrix is observed possibly due to interactions between gas molecules and the biopolymer chains and/or ionic liquid, resulting not only in a disorder or phase change of the LC, but also in a spatial redistribution of the LC-ionic liquid droplets.[42,43] When compared to nonpolar compounds, a longer LC response time to the vapors was detected (Figure 15).

The sensitivity of LC-based systems can be improved by using nanomaterials, such as CNTs, as dopant agents (Figure 16). The dispersion of CNTs in LC matrices leads to aligned assemblies of LC and CNTs, due to the LC orientational order that can be imposed on CNTs. Furthermore, CNTs form conductive networks within CNT–LC hybrid materials, which can be altered by changing the orientation of CNT–LCs.

Lai et al.[144,145] prepared a polymer dispersed liquid crystal, 5CB, doped with CNTs, in which the polymer film supports the LC droplets. The CNTs are entrapped inside both the polymer and the droplet, overall forming a hybrid system which is very sensitive to any variation of director orientation (Figure 16a). The hybrid sensing film is spin coated into planar interdigitated electrode pairs. When the sensing material is exposed to a target volatile organic compound (DMMP[145] or acetone[144]), a reorientation of the LC molecules and, consequently, the restructure of the CNT networks occurs. The presence of the VOC

can be detected by measuring the changes in the electrical resistance of the hybrid sensing material. The sensitivity of this mechanism increases with decreasing the film thickness. Nonetheless, the film must be thick enough to allow for the droplet formation, being the film's optimal thickness for the detection of acetone vapor estimated at 6.7 μm[144] (Figure 16c).

3.5 Chiral Liquid Crystal Systems

The incorporation of chiral LC systems in gas sensing devices (Table 5) typically takes advantage of the fact that the presence of solvent vapors can result in either a change of the helical twisting power of the chiral dopant due to reaction with the analyte or physical swelling of the system with a change of order in the LC phase, which ultimately changes the helical pitch due to absorption of the analyte. Both mechanisms lead to a shift of the selective reflection band which can be observed with the naked eye[146–152] (Figure 17).

Mujahid et al.[153] combined both optical and mass-sensitive detection techniques to acquire deeper knowledge on the sensing mechanism. The exposure of ethanol, tetrahydrofuran, chloroform, and tetrachloroethylene molecules on a chiral biphenyl-based LC sensing material results in a disturbance of the pitch length, leading to a blue-shift which can be linearly correlated with the molecular mass of the solvent examined. Polar analytes such as tetrachloroethylene and chloroform seem to be more strongly intercalated within the LC than polar solvents such as ethanol, in a concentration range up to 0.5% solvent vapor in the air. The authors also showed that embedding the chiral LC in a cross-linked polystyrene matrix can increase selectivity when compared to the pure LC material.

Chang et al.[154] used the nematic eutectic mixture, E7 doped with chiral agents, S1011 (17 wt%, Merck) and DBD (2 wt%, WeiFlex), as a sensing material for acetone and toluene vapors. As the organic molecules diffuse through the system, a redshift in the reflection spectra is observed due to a swelling of the chiral pitch. When a certain threshold amount of analyte is absorbed, a phase transition occurs, and the structure becomes isotropic. Shift differences are due to the different molecular polarities of acetone and toluene, since high molecular polarity molecules cause a greater shift. Due to a favorable interaction with the cyano group of the LC, acetone presented a stronger and faster response. This mechanism was also the basis of another novel sensing device by the authors in 2012,[155] using hydrogen-bridged chiral LC polymer networks with defined porosity to distinguish between methanol and ethanol.

Similar to the principle discussed in Section 3.3., dopant materials can also be used to induce or enhance sensitivity and/or selectivity toward a specific gas molecule. Aksimentyeva et al.,[156] Sushynskyi et al.,[157] and Vistak et al.[158] used chiral LCs doped with magnetite nanoparticles. Magnetite exhibits a high affinity for carbon monoxide, due to the presence of iron atoms in the oxidation states +2 and +3, similar to the case of a hemoglobin molecule, hence acting as a sensing element. This causes a distortion of the ordering within the chiral LC system, specifically an increase of the chiral pitch, leading to changes in the transmission spectra. It was also suggested by all three works that these changes were more prominent at high concentrations of carbon monoxide, roughly up to 100 mg m^{-3}. Chang et al.[159] studied a hybrid material, composed by a chiral LC (the system

described in [154]) and CNTs, for the detection of both low and high concentrations of acetone vapors (up to 550 ppm). At low concentrations (up to 140 ppm), the detection is achieved through a color change of the chiral LC system due to swelling of the chiral helix and ultimately a total disruption of the LC assembly. At higher concentrations (160–550 ppm), the hybrid system forms conducting networks, due to the CNTs branching out and the detection of acetone can be realized via monitoring changes in the electrical resistance of the system.

Another approach to using chiral dopants is based on the principle that, upon reaction with a specific analyte, the dopant will respond with either a chemical or a supramolecular way, leading to changes in the reflected color.[99,160] For example, Cachelin et al.[161] have recently developed a time-integrating sensor, which can serve as a chemical dosimeter by measuring the total exposure to an analyte over a given time frame. In their work, they described an acetone vapor detection system, based on a film of E7 doped with tetraaryl-1,3-dioxolane (TADDOL)–phenylhydrazine complex. The chiral nematic LC films were exposed 1000 parts per million by volume (ppmv) of acetone vapors for 2 h and show a red shift, caused by an irreversible reaction between the dopant and the gas analyte. Han et al. [162] also used E7 doped with an optically pure diamine–TADDOL derivative complex (1·3 in Figure 18) to detect carbon dioxide in real time, since diamines reversibly react with carbon dioxide forming carbamate, causing a shift in the reflection band from 637 nm (red) to 495 nm (green). In the same study, E7 was also doped with a chiral binaphthyl dithiol derivative and a nonresponsive codopant for oxygen exposure detection over time. A color change was observed from green (542 nm) to orange (600 nm) due to an irreversible oxidation reaction of dithiol to disulfide.

Shibaev et al.[163] in their work explored the possibility of monitoring color changes in LC droplets observed under the microscope, rather than isotropization transitions, in order to decrease the detection limit of the gas analytes tested. They employed 5CB, MBBA and mixtures of 5CB/MBBA doped with a chiral additive (ethylbenzylamine). Nematic droplets were deposited on surfaces treated to promote a planar orientation, whereas chiral droplets were deposited on surfaces for homeotropic alignment. For the nematic droplets, VOCs detection was achieved via the observation and analysis of the interference colors formed in the periphery of each droplet. This could be achieved because both the LC orientation and order parameter can be more influenced by the gas presence in the thinner parts of the droplets. It was found that the absorption of gas molecules leads to shifts in the interference colors generated in the droplets' fringes, above certain analyte concentrations. Similarly, in the case of chiral droplets, they exploited brightness and contrast changes in the corresponding fingerprint optical texture (the shape and structure of the texture remained unaffected upon exposure) to detect vapors of small analyte concentrations.

Finally, a prototype olfaction system (electronic nose) was reported by Shibaev et al.,[48] implementing an array of six different chiral mixtures (containing MBBA, derivatives of cholesterol and a glass forming chiral oligomer), in the form of droplets, with variable viscosities. Each droplet had a different response to VOCs (cyclohexane and acetic acid) depending on the system's viscosity. They concluded that monitoring color fluctuation and light reflection changes is sufficient enough for the detection of small VOCs concentrations

(0.1–2 μL/200 cm^3), whereas for larger analyte concentrations (5–8 μL/200 cm^3, Figure 19) detection is based on isotropization transitions or entire droplet color changes. Recently, they also explored the atomic force microscopy (AFM) technique as a means to monitor the response of a chiral LC system to volatile vapors.[164] The glass-forming chiral oligomer Wacker deposited on small glass plates was the system under study. The LC was exposed to vapors of water, ethanol, and toluene and responded only to toluene. AFM investigation before and after exposure showed a reconstruction of the spiral focal conic surface structure at the presence of toluene vapors.

4 Transduction Methods in Liquid Crystal-Based Sensors

The most crucial feature of LC-based sensing systems is that they are sensitive to perturbations occurring in their molecular order or orientation, resulting in changes of their properties, for example optical or electrical and yielding output measurable signals. As such, distinct transduction methods can be coupled to LC-based platforms.

For example, in the case of nematic LCs, due to changes in the transmitted light intensity through the LC medium, gas detection can be realized through polariscopy[100,101] or POM.[116–121] For chiral LCs[146,147,153] or LCs doped with magnetite nanoparticles,[156–158] LC-VOCs or gas interaction can be detected by spectroscopy techniques due to changes in the absorption, transmission and/or reflection spectra of the sensing materials. As mentioned in Section 3.5., in chiral systems the shift of the selective reflection band occurs within the visible spectrum allowing for a quick and direct detection with the naked eye.[146,150,160,162] Additionally, gas or VOC interactions were also characterized by Fourier-transform infrared spectroscopy (FTIR)[149,160,162] or Raman spectroscopy.[140] Other transduction methods include the use of custom-made devices,[42,94,109,127,142] SPR[135] (used to detect subtle changes in LC birefringence), or quartz crystal microbalance[153] (used to detect mass changes when chiral LCs were coated on acoustic devices). As discussed in Section 3.6, discotic LCs films exhibit changes in their surface conductivity upon gas exposure.[104–106] Last, in the case of polymer dispersed LCs doped with CNTs the detection was achieved via measuring changes in the electrical conductivity of the sensing films.[144,145]

Of special interest is the case of gas sensor devices that exploit the birefringence of LCs, typically measuring the intensity of light transmitted through the LC medium when placed between crossed polarizers. For example, Sridharamurthy et al.[108] demonstrated a detection method consisting of two crossed polarizing films placed on top and bottom of the sensing material, by using a white light as illumination source and a digital camera connected to a computer, to continuously monitor the presence or absence of analytes. Yang et al.[109] used a digital camera, with a polarizing lens, to monitor the LC state and another polarizer placed between the white light source and the sensing material. The final analysis was performed by converting all images to a gray scale of intensities and their luminosities were subsequently analyzed by Photoshop. Hussain et al.,[42] Semeano et al.,[142] and more recently Esteves et al.[43] used a custom-made device[165] where the total intensity of light, generated from a light-emitting diode and transmitted through crossed polarizers, was converted into an electrical signal by using a light-dependent resistor. Reyes et al.[44] and Wang et al.[94] detection methods were based on placing the sensing materials between

crossed polarizers, allowing for the detection of changes of the transmitted light with the naked eye.

Ho et al.[112] manufactured an optical waveguide sensor and used an infrared camera to register the waveguide output profile before and after ethanol exposure, yielding a strong waveguide output and no output respectively. Some groups have combined both electrical and optical responses in their devices, such as Chang et al.[159] There, they implemented a chiral LC doped with CNTs and used a POM equipped with a spectrometer to obtain optical images and analyze the shift in the reflected color. Additionally, they placed the LC compound on a cell with comb-like electrodes of conductive silver and with the use of a DC resistance meter they measured the electrical resistance of the system to trace any differences during gas exposure.

5 Conclusion and Future Perspectives

Liquid crystals are anisotropic elastic materials composed by mobile molecules, similar to isotropic liquids and capable of long-range orientational ordering, as in crystal solids. They are optically, electrically, and magnetically active materials. Specifically, orientational and ordering changes can be induced upon application or alteration of electric and magnetic fields, or in response to stimuli such as shear, temperature and light, making them attractive candidates for a plethora of technologies.[17,166]

Liquid crystal ordering can also be affected by the presence of chemical analytes, interacting either via the imposed surface boundaries or directly with the LC mesophase. In both cases, the net result is the disruption of the initial molecular order and manipulation of the director alignment, an effect that can be usually followed, for example, by changes in the optical properties of the LC. In this context, a new and exciting field of applications has been, and still is, explored by researchers over the last years: the development of cheap and fast sensors for chemical and biological sensing, both in liquid and gas phases.[15,167,168]

A key requirement is to achieve stable, yet stimuli-responsive and dynamic molecular orientation. In this sense, different geometries and boundary conditions have been attempted; starting from those relative to display applications, and further exploring new, unconventional and exotic even approaches, including droplets, shells, fibers, and colloidal systems.[90] Research achievements and developments so far strongly suggest that the future potential for LC gas sensing platforms is very promising due to the maturity that LC-based technologies has reached, the multisensing capabilities of LCs to chemical and physical cues, as well as their easy integration with several other multifunctional and flexible materials.

Only a few LC-based sensor technologies have been commercialized and patented so far,[169] since the field is still at an early stage. In order to further progress and reach a mass production and commercial level, certain research directions should be explored.[170] For example, a critical mater is the development of improved and targeted LC systems, through rational design, in order to achieve enhanced selectivity and sensitivity toward gas and VOC analytes. This challenge could be addressed through computational chemistry,[138] leading to

Europe PMC Funders Author Manuscripts

the discovery of novel chemoresponsive systems and also providing valuable feedback to experimental researchers. For example, Szilvasi et al.[138] synthesized the fluorinated cyanobiphenyl LC system discussed in Section 3.3, based on a computational model they developed, in order to achieve a better response to DMMP.

Another challenge that needs to be addressed is the implementation of a systematic and comprehensive procedure for the accurate interpretation, classification and prediction of possible patterns of the large amount of data, generated from sensing experiments. This task is time consuming and not humanly feasible for a commercial device. Machine learning-based methodologies can eliminate the human factor and have proven to exhibit a tremendous potential.[43,121] Esteves et al.[43] developed and implemented an automatic classifier algorithm based on support vector machines for processing the data acquired during the exposure of gelatin hybrid gels to 11 VOCs from distinct chemical classes. This approach led to a highly accurate (>97%) classification of the VOCs in study. In addition, Cao et al.[121] employed a similar approach to classify experimental data provided by a LC-based sensor they developed, using as input POM images during VOCs exposure.

Overall, research reports strongly suggest that there are several advantages to the implementation of LCs in gas sensing devices as they can operate at room temperature, the device selectivity can be tuned according to the chemistry of the interface in contact with the LC, and most importantly, they do not require complex instrumentation. Hence the devices developed can be easy to assemble, portable and simple to use. It is also notable that LCs can be easily incorporated or confined in other rigid or flexible organic and inorganic materials,[171] which is very promising for future developments in artificial olfaction coupled to wireless and wearable optoelectronic devices.

Acknowledgements

The authors acknowledge funding from the European Research Council through the grant reference SCENT-ERC-2014-STG-639123 (2015-2020). The authors also acknowledge funding from the Applied Molecular Biosciences Unit - UCIBIO (UIDB/04378/2020), and the PhD grant to CE (SFRH/BD/113112/2015), which are financed by national funds from Fundação para a Ciência e Tecnologia. The authors greatly acknowledge the support from Dr. David Roberts for language editing and image design.

Biographies

Carina Esteves is a MIT-Portugal Ph.D. student in bioengineering systems, currently finishing her Ph.D. thesis under the guidance of Prof. Cecilia Roque in the Biomolecular Engineering Lab, UCIBIO, Faculdade Ciências e Tecnologia, Universidade Nova de Lisboa (FCT-NOVA), Portugal. Carina received her degree in applied chemistry – profile

biotechnology and a MSc in biotechnology both from FCT-NOVA. From 2010 to 2015, she worked as a researcher at Mecwins S.A., Spain. Her Ph.D. project is focused on the development of novel self-assembling materials for gas-sensing applications.

Efthymia Ramou has a M.Sc. and a Ph.D. in physics, with a focus on novel liquid crystal materials, from the University of Patras, Greece. Currently, she is a postdoctoral research fellow in Cecilia Roque's Biomolecular Engineering Lab at UCIBIO, Faculdade de Ciências e Tecnologia, Universidade Nova de Lisboa, Portugal. Efthymia's research project is focused on the development of gas-sensitive liquid-crystal-based materials and the impact of the liquidcrystal component on the self-assembly of the system. Her research interests include mesophases with modulated structure and liquid-crystal materials for optoelectronic devices.

Ana Cecília Afonso Roque is an associate professor with Habilitation in Bioengineering and head of the Biomolecular Engineering Lab at UCIBIO, Faculdade de Ciências e Tecnologia, Universidade Nova de Lisboa, Portugal. She holds a degree in chemical engineering and a Ph.D. in biotechnology from Instituto Superior Técnico, Universidade de Lisboa. Cecília has been a Visiting Scholar at the University of Cambridge, UK and a post-doctoral researcher at the University of Cambridge and at INESC-MN, Lisboa. She was a visiting professor at the University of Nantes, France (2011) and the University of São Paulo, Brazil (2015–2018). Cecília's group focuses on the design and development of affinity functional materials, particularly for noninvasive sensing applications.

References

[1]. Reinitzer F. Monatsh Chem - Chem Mon. 1888; 9:421.

[2]. Dunmur, D, Sluckin, T. Soap, Science, and Flat-Screen TVs: A History of Liquid Crystals; Structure and Properties of Liquid Crystals. Oxford University Press; Oxford: 2014.

[3]. Bremer M, Kirsch P, Klasen-Memmer M, Tarumi K. Angew Chem - Int Ed. 2013; 52:8880.

[4]. Bailey J, Morgan P, Gleeson HF, Jones JC. Crystals. 2018; 8:29.

[5]. Manna SK, Le-Gall S, Dupont L, Li G. J Mol Liq. 2016; 220:161. [PubMed: 29225387]

[6]. De J, Yang WY, Bala I, Gupta SP, Yadav RAK, Dubey DK, Chowdhury A, Jou JH, Pal SK. ACS Appl Mater Interfaces. 2019; 11:8291. [PubMed: 30707013]

Europe PMC Funders Author Manuscripts

[7]. Kumar M, Kumar S. Polym J. 2017; 49:85.

[8]. O'Neill M, Kelly SM. Adv Mater. 2011; 23:566. [PubMed: 21274907]

[9]. Fernandes SN, Almeida PL, Monge N, Aguirre LE, Reis D, de Oliveira CLP, Neto AMF, Pieranski P, Godinho MH. Adv Mater. 2017; 29

[10]. Chang CM, Lin YH, Srivastava AK, Chigrinov VG. Sci Rep. 2018; 8

[11]. Kim YK, Wang X, Mondkar P, Bukusoglu E, Abbott NL. Nature. 2018; 557:539. [PubMed: 29743674]

[12]. Zhou L, Hu Q, Kang Q, Fang M, Yu L. Langmuir. 2019; 35:461. [PubMed: 30576146]

[13]. Schwartz M, Lenzini G, Geng Y, Ronne PB, Ryan PYA, Lagerwall JPF. Adv Mater. 2018; 30

[14]. Yano K, Itoh Y, Araoka F, Watanabe G, Hikima T, Aida T. Science. 2019; 363:161. [PubMed: 30630928]

[15]. Hussain A, Pina AS, Roque ACA. Biosens Bioelectron. 2009; 25:1. [PubMed: 19477113]

[16]. Carlton RJ, Hunter JT, Miller DS, Abbasi R, Mushenheim PC, Tan LN, Abbott NL. Liq Cryst Rev. 2013; 1:29.

[17]. Bukusoglu E, Bedolla Pantoja M, Mushenheim PC, Wang X, Abbott NL. Annu Rev Chem Biomol Eng. 2016; 7:163. [PubMed: 26979412]

[18]. Popov N, Honaker LW, Popova M, Usol'tseva N, Mann EK, Jakli A, Popov P. Materials. 2018; 11:20.

[19]. Lowe AM, Abbott NL. Chem Mater. 2012; 24:746. [PubMed: 22563142]

[20]. Wang D, Park SY, Kang IK. J Mater Chem C. 2015; 3:9038.

[21]. Schenning, A, Crawford, GP, Broer, DJ, editors. Liquid Crystal Sensors. CRC Press; Boca Raton, FL: 2017.

[22]. Munir S, Park SY. Sens Actuators B, Chem. 2018; 257:579.

[23]. Wei Y, Jang CH. J Mater Sci. 2015; 50:4741.

[24]. Popov P, Mann EK, Jakli A. J Mater Chem B. 2017; 5:5061. [PubMed: 32264091]

[25]. Bao P, Paterson DA, Harrison PL, Miller K, Peyman S, Jones JC, Sandoe J, Evans SD, Bushby RJ, Gleeson HF. Lab Chip. 2019; 19:1082. [PubMed: 30785139]

[26]. Lowe AM, Ozer BH, Bai Y, Bertics PJ, Abbott NL. ACS Appl Mater Interfaces. 2010; 2:722. [PubMed: 20356273]

[27]. Wu PC, Karn A, Lee MJ, Lee W, Chen CY. Dye Pigm. 2018; 150:73.

[28]. Popov P, Honaker LW, Kooijman EE, Mann EK, Jakli AI. Sens Bio-Sens Res. 2016; 8:31.

[29]. Khan M, Khan AR, Shin JH, Park SY. Sci Rep. 2016; 6

[30]. Sivakumar S, Wark KL, Gupta JK, Abbott NL, Caruso F. Adv Funct Mater. 2009; 19:2260.

[31]. Zafiu C, Hussain Z, Kupcu S, Masutani A, Kilickiran P, Sinner EK. Biosens Bioelectron. 2016; 80:161. [PubMed: 26827146]

[32]. Luk YY, Campbell SF, Abbott NL, Murphy CJ. Liq Cryst. 2004; 31:611.

[33]. Hussain Z, Zafiu C, Kupcu S, Pivetta L, Hollfelder N, Masutani A, Kilickiran P, Sinner EK. Biosens Bioelectron. 2014; 56:210. [PubMed: 24508543]

[34]. [accessed: September 2019] Gas Sensor Market Size and Share, Global Industry Report, 2019–2025. https://www.grandviewresearch.com/industry-analysis/gas-sensors-market

[35]. Chehri, A; Farjow, W; Mouftah, HT; Fernando, X. Canadian Conf. on Electrical and Computer Engineering (CCECE); Piscataway, NJ: IEEE; 2011. 001532

[36]. Manna, S; Bhunia, SS; Mukherjee, N. Int. Conf. Recent Advances and Innovations in Engineering (ICRAIE 2014); Piscataway, NJ: IEEE; 2014. 1

[37]. van Hooren MRA, Leunis N, Brandsma DS, Dingemans AMC, Kremer B, Kross KW. Eur Arch Otorhinorlaryngol. 2016; 273:3897.

[38]. Zampolli S, Elmi I, Ahmed F, Passini M, Cardinali GC, Nicoletti S, Dori L. Sens Actuators B, Chem. 2004; 101:39.

[39]. Khan A, Schaefer D, Tao L, Miller DJ, Sun K, Zondlo MA, Harrison WA, Roscoe B, Lary DJ. Remote Sens. 2012; 4:1355.

[40]. Dey A. Mater Sci Eng B. 2018; 229:206.

[41]. Park SJ, Park CS, Yoon H. Polymers. 2017; 9:155.
[42]. Hussain A, Semeano ATS, Palma SICJ, Pina ASP, Almeida J, Medrado BFF, Padua ACCS, Carvalho AL, Dionisio M, Li RWC, Gamboa H, et al. Adv Funct Mater. 2017; 27
[43]. Esteves C, Santos GMC, Alves C, Palma SICJ, Porteira AR, Filho J, Costa HMA, Alves VD, Morais BM, Ferreira I, Gamboa H, et al. Mater Today Bio. 2019; 1
[44]. Reyes CG, Sharma A, Lagerwall JPF. Liq Cryst. 2016; 43:1986.
[45]. Szilvasi T, Bao N, Yu H, Twieg RJ, Mavrikakis M, Abbott NL. Soft Matter. 2018; 14:797. [PubMed: 29308482]
[46]. Sen A, Kupcho KA, Grinwald BA, Vantreeck HJ, Acharya BR. Sens Actuators B, Chem. 2013; 178:222. [PubMed: 23526230]
[47]. Bedolla Pantoja MA, Abbott NL. ACS Appl Mater Interfaces. 2016; 8:13114. [PubMed: 27070511]
[48]. Shibaev PV, Carrozzi D, Vigilia L, DeWeese H. Liq Cryst. 2019; 46:1309.
[49]. Demus, D, Goodby, J, Gray, GW, Spiess, HW, Vill, V, editors. Handbook of Liquid Crystals. Vol. 1. Wiley-VCH; Weinheim, Germany: 1998.
[50]. de Gennes, PG, Prost, J. The Physics of Liquid Crystals. Clarendon Press; Oxford, UK: 1995.
[51]. Tschierske C. Chem Soc Rev. 2007; 36:1930. [PubMed: 17982518]
[52]. Collings, PJ, Hird, M. Introduction to Liquid Crystals: Chemistry and Physics. Taylor & Francis; London, UK: 1997.
[53]. Pelzl G, Wirth I, Weissflog W. Liq Cryst. 2001; 28:969.
[54]. Reddy RA, Tschierske C. J Mater Chem. 2006; 16:907.
[55]. Takezoe H, Takanishi Y. Jpn J Appl Phys. 2006; 45:597.
[56]. Etxebarria J, Ros MB. J Mater Chem. 2008; 18:2919.
[57]. Goodby, JW, Collings, PJ, Kato, T, Tschierske, C, Gleeson, H, Raynes, P. Handbook of Liquid Crystals. Wiley−VCH; Weinheim, Germany: 2014.
[58]. [accessed: January 2014] https://www.dupont.com/what-is-kevlar.html
[59]. Griffin AC, Britt TR. J Am Chem Soc. 1981; 103:4957.
[60]. Blumstein A, Thomas O. Macromolecules. 1982; 15:1264.
[61]. Panov VP, Vij JK, Mehl GH. Liq Cryst. 2017; 44:147.
[62]. Mandle RJ. Chem - A Eur J. 2017; 23:8771.
[63]. Imrie, CT, Luckhurst, GR. Handbook of Liquid Crystals. Goodby, JW, Collings, PJ, Kato, T, Tschierske, C, Gleeson, H, Rayne, P, editors. Vol. 7. Wiley-VCH; Weinheim Germany: 2014.
[64]. Chandrasekhar, S. Liquid Crystals. Cambridge University Press; Cambridge: 1992.
[65]. Freiser MJ. Phys Rev Lett. 1970; 24:1041.
[66]. Tschierske C, Photinos DJ. J Mater Chem. 2010; 20:4263.
[67]. van den Pol E, Petukhov AV, Thies-Weesie DME, Byelov DV, Vroege GJ. Phys Rev Lett. 2009; 103
[68]. Vroege GJ. Liq Cryst. 2014; 41:342.
[69]. Yu LJ, Saupe A. Phys Rev Lett. 1980; 45:1000.
[70]. Madsen LA, Dingemans TJ, Nakata M, Samulski ET. Phys Rev Lett. 2004; 92
[71]. Panov VP, Nagaraj M, Vij JK, Panarin YP, Kohlmeier A, Tamba MG, Lewis RA, Mehl GH. Phys Rev Lett. 2010; 105
[72]. Cestari M, Diez-Berart S, Dunmur DA, Ferrarini A, de La Fuente MR, Jackson DJB, Lopez DO, Luckhurst GR, Perez-Jubindo MA, Richardson RM, Salud J, et al. Phys Rev E - Nonlinear Stat, Soft Matter Phys. 2011; 84
[73]. Borshch V, Kim YK, Xiang J, Gao M, Jakli A, Panov VP, Vij JK, Imrie CT, Tamba MG, Mehl GH, Lavrentovich OD. Nat Commun. 2013; 4
[74]. Ramou E, Ahmed Z, Welch C, Karahaliou PK, Mehl GH. Soft Matter. 2016; 12:888. [PubMed: 26549345]
[75]. Mandle RJ. Soft Matter. 2016; 12:7883. [PubMed: 27722733]
[76]. Ramou E, Welch C, Hussey J, Ahmed Z, Karahaliou PK, Mehl GH. Liq Cryst. 2018; 45:1929.

[77]. Dierking, I. Textures of Liquid Crystals. Wiley-VCH Verlag GmbH & KGaA Co; Weinheim, Germany: 2003.

[78]. Lagerwall JPF, Giesselmann F. ChemPhysChem. 2006; 7:20. [PubMed: 16404767]

[79]. Sluckin, TJ, Dunmur, DA, Stegemeyer, H, editors. Crystals That Flow: Classic Papers from the History of Liquid Crystals. Taylor & Francis; London: 2004.

[80]. Selinger JV. Liq Cryst Rev. 2018; 6:129.

[81]. Takatoh, K, Hasegawa, M, Koden, M, Itoh, N, Hasegawa, R, Sakamoto, M. Alignment Technologies and Applications of Liquid Crystal Devices. Taylor & Francis; London: 2005.

[82]. Parry-Jones, L. Handbook of Visual Display Technology. Chen, J, Cranton, W, Fihn, M, editors. Springer, Cham; Switzerland: 2016.

[83]. Miller DS,Carlton RJ, Mushenheim PC, Abbott NL. Langmuir. 2013; 29:3154. [PubMed: 23347378]

[84]. Rapini A, Papoular M. J Phys Colloq. 1969; 30:C4.

[85]. Drzaic, PS. Liquid Crystal Dispersions. Ong, HL, editor. World Scientific; Singapore: 1995. 99

[86]. Kurik MV, Lavrentovich OD. Usp Fiz Nauk. 1988; 31:196.

[87]. Miller DS, Wang X, Abbott NL. Chem Mater. 2014; 26:496. [PubMed: 24882944]

[88]. Volovik GE, Lavrentovich OD. Sov Phys - JETP. 1983; 58:1159.

[89]. Lopez-Leon T, Fernandez-Nieves A. Colloid Polym Sci. 2011; 289:345.

[90]. Urbanski M, Reyes CG, Noh JH, Sharma A, Geng Y, Subba Rao Jampani V, Lagerwall JPF. J Phys: Condens Matter. 2017; 29

[91]. Gupta JK, Zimmerman JS, De Pablo JJ, Caruso F, Abbott NL. Langmuir. 2009; 25:9016. [PubMed: 19719217]

[92]. Lavrentovich OD. Sov Phys - JETP. 1986; 64:984.

[93]. Lee HG, Munir S, Park SY. ACS Appl Mater Interfaces. 2016; 8:26407. [PubMed: 27618511]

[94]. Wang J, Jakli A, West JL. J Mol Liq. 2018; 267:490.

[95]. Williams C, Pieranski P, Cladis PE. Phys Rev Lett. 1972; 29:90.

[96]. Ondris-Crawford RJ, Crawford GP, Zumer S, Doane JW. Phys Rev Lett. 1993; 70:194. [PubMed: 10053726]

[97]. Scharf, T. Polarized Light in Liquid Crystals and Polymers. John Wiley & Sons, Inc; New York: 2007.

[98]. Shvetsov SA, Rudyak VY, Emelyanenko AV, Boiko NI, Zhang YS, Liu JH, Khokhlov AR. J Mol Liq. 2018; 267:222.

[99]. Ferganson JL, Goldberg NN, Jones CH, Rush RS, Scala LC. Detection of Liquid Crystal Gases (Reactive Materials) - Technical Report No. RADC-TR-64-569. 1965

[100]. Novak TJ, Poziomek EJ, Mackay RA. Anal Lett. 1972; 5:187.

[101]. Poziomek EJ, Novak TJ, Mackay RA. Mol Cryst Liq Cryst. 1974; 27:175.

[102]. Adgate JL, Bartekova A, Raynor PC, Griggs JG, Ryan AD, Acharya BR, Volkmann CJ, Most DD, Lai S, Bonds MD. J Environ Monit. 2009; 11:49. [PubMed: 19137139]

[103]. Mulder DJ, Schenning APHJ, Bastiaansen CWM. J Mater Chem C. 2014; 2:6695.

[104]. Clements J, Boden N, Gibson TD, Chandler RC, Hulbert JN, Ruck-Keene EA. Sens Actuators: B Chem. 1998; 47:37.

[105]. Wright JD, Roisin P, Rigby GP, Nolte RJM, Cook MJ, Thorpe SC. Actuators Sens, B. 1993; 13:276.

[106]. Boden N, Bushby RJ, Clements J, Movaghar B. J Mater Chem. 1999; 9:2081.

[107]. Sridharamurthy, SS, Cadwell, KD, Abbott, NL, Jiang, HR. IEEE Sensors: IEEE; Piscataway, NJ: 2007. 1044–1047.

[108]. Sridharamurthy SS, Cadwell KD, Abbott NL, Jiang H. Smart Mater Struct. 2008; 17

[109]. Yang KL, Cadwell K, Abbott NL. Actuators Sens, B. 2005; 104:50.

[110]. Cadwell KD, Alf ME, Abbott NL. J Phys Chem B. 2006; 110

[111]. Bungabong ML, Ong PB, Yang KL. Sens Actuators B Chem. 2010; 148:420.

[112]. Ho WF, Chan HP, Yang KL. IEEE Sens J. 2013; 13:2521.

[113]. Niu X, Zhong Y, Chen R, Wang F, Luo D. Opt Express. 2017; 25
[114]. Wang PH, Yu JH, Zhao YB, Li ZJ, Li GQ. Sens Actuators B Chem. 2011; 160:929.
[115]. Shah RR, Abbott NL. Science. 2001; 293:1296. [PubMed: 11509724]
[116]. Xu H, Bi X, Ngo X, Yang KL. Analyst. 2009; 134:911. [PubMed: 19381384]
[117]. Hunter JT, Pal SK, Abbott NL. ACS Appl Mater Interfaces. 2010; 2:1857.
[118]. Hunter JT, Abbott NL. Sens Actuators, B. 2013; 183:71.
[119]. Vantreeck HJ, Most DR, Grinwald BA, Kupcho KA, Sen A, Bonds D, Acharya BR. Sens Actuators B, Chem. 2011; 158:104.
[120]. Cheng D, Sridharamurthy SS, Hunter JT, Park JS, Abbott L, Jiang H. J Microelectromech Syst. 2009; 18:973.
[121]. Cao Y, Yu H, Abbott NL, Zavala VM. ACS Sens. 2018; 3:2237. [PubMed: 30289249]
[122]. Roling LT, Scaranto J, Herron JA, Yu H, Choi S, Abbott NL, Mavrikakis M. Nat Commun. 2016; 7
[123]. Acharya BR. Laser Focus World. 2010; 46:68.
[124]. Bi X, Yang KL. Sens Actuators B, Chem. 2008; 134:432.
[125]. Cadwell KD, Lockwood NA, Nellis BA, Alf ME, Willis CR, Abbott L. Sens Actuators B, Chem. 2007; 128:91.
[126]. Yang KL, Cadwell K, Abbott NL. J Phys Chem. B. 2004; 108
[127]. Robinson SE, Grinwald BA, Bremer LL, Kupcho KA, Acharya BR, Owens PD. J Occup Environ Hyg. 2014; 11:741. [PubMed: 24766440]
[128]. Szilvasi T, Bao N, Nayani K, Yu H, Rai P, Twieg RJ, Mavrikakis M, Abbott NL. Angew Chem, Int Ed. 2018; 57:9665.
[129]. Hunter JT, Abbott NL. ACS Appl Mater Interfaces. 2014; 6:2362. [PubMed: 24369715]
[130]. Shah RR, Abbott NL. Langmuir. 2003; 19:275.
[131]. Shah RR, Abbott NL. J Am Chem Soc. 1999; 121
[132]. Thomas CR, Houston JE, Crooks RM, Kim T, Michalske TA. Langmuir. 1995; 117:3830.
[133]. Nayani K, Rai P, Bao N, Yu H, Mavrikakis M, Twieg RJ, Abbott NL. Adv Mater. 2018; 30
[134]. Drapp B, Pauluth D, Krause J, Gauglitz G. Fresenius' J Anal Chem. 1999; 364:121.
[135]. Kieser B, Pauluth D, Gauglitz G. Anal Chim Acta. 2001; 434:231.
[136]. Shibaev PV, Wenzlick M, Murray J, Tantillo A, Howard-Jennings J. Adv Condens Matter Phys. 2015; 2015:1.
[137]. Ohzono T, Yamamoto T, Fukuda JI. Nat Commun. 2014; 5
[138]. Szilvasi T, Roling LT, Yu H, Rai P, Choi S, Twieg RJ, Mavrikakis M, Abbott NL. Chem Mater. 2017; 29:3563.
[139]. Ding X, Yang KL. Sens Actuators B, Chem. 2012; 173:607.
[140]. Nandi R, Singh SK, Singh HK, Singh B, Singh RK. Chem Phys Lett. 2014; 614:62.
[141]. Pal SK, Acevedo-Velez C, Hunter JT, Abbott NL. Chem Mater. 2010; 22:5474.
[142]. Semeano ATS, Maffei DF, Palma SICJ, Li RWC, Franco DGM, Roque ACA, Gruber J. Food Control. 2018; 89:72. [PubMed: 29503510]
[143]. Hu Q, Jang C. Soft Matter. 2013; 9:5779.
[144]. Lai YT, Kuo JC, Yang YJ. Sens Actuators A, Phys. 2014; 215:83.
[145]. Lai YT, Kuo JC, Yang YJ. Appl Phys Lett. 2013; 102
[146]. Sutarlie L, Qin H, Yang KL. Analyst. 2010; 135:1691. [PubMed: 20583347]
[147]. Winterbottom DA, Narayanaswamy R, Raimundo IM. Sens Actuators B, Chem. 2003; 90:52.
[148]. Dickert FL, Haunschild A, Hofmann P. Fresenius' J Anal Chem. 1994; 350:577.
[149]. Stumpel JE, Wouters C, Herzer N, Ziegler J, Broer DJ, Bastiaansen CWM, Schenning APHJ. Adv Opt Mater. 2014; 2:459.
[150]. Kirchner N, Zedler L, Mayerhofer TG, Mohr GJ. Chem Commun. 2006; 1512
[151]. Tang J, Fang J, Liang Y, Zhang B, Luo Y, Liu X, Li Z, Cai X, Xian J, Lin H, Zhu W, et al. Sens Actuators B, Chem. 2018; 273:1816.

[152]. Kek KJ, Lee JJZ, Otono Y, Ishihara S. J Soc Inf Disp. 2017; 25:366.
[153]. Mujahid A, Stathopulos H, Lieberzeit PA, Dickert FL. Sensors. 2010; 10:4887. [PubMed: 22399912]
[154]. Chang CK, Kuo HL, Tang KT, Chiu SW. Appl Phys Lett. 2011; 99
[155]. Chang CK, Bastiaansen CWM, Broer DJ, Kuo HL. Macro-molecules. 2012; 45:4550.
[156]. Aksimentyeva O, Mykytyuk Z, Fechan A, Sushynskyy O, Tsizh B. Mol Cryst Liq Cryst. 2014; 589:83.
[157]. Sushynskyi O, Vistak M, Gotra Z, Andriy F, Mikityuk Z. Proc SPIE - Int Soc Opt Eng. 2014; 9127
[158]. Vistak M, Sushynskyi O, Mykytyuk Z, Aksimentyeva O, Semenova Y. Sens Actuators A, Phys. 2015; 235:165.
[159]. Chang CK, Chiu SW, Kuo HL, Tang KT. Appl Phys Lett. 2012; 100
[160]. Sutarlie L, Lim JY, Yang KL. Anal Chem. 2011; 83:5253. [PubMed: 21630648]
[161]. Cachelin P, Green JP, Peijs T, Heeney M, Bastiaansen CWM. Adv Opt Mater. 2016; 4:592.
[162]. Han Y, Pacheco K, Bastiaansen CWM, Broer DJ, Sijbesma RP. J Am Chem Soc. 2010; 132:2961. [PubMed: 20148584]
[163]. Shibaev PV, Wenzlick M, Murray J, Tantillo A, Howard-Jennings J. Mol Cryst Liq Cryst. 2015; 611:94.
[164]. Shibaev PV, Carrozzi D, Vigilia L, Panariti A, Schwartz GA. Liq Cryst. 2019; 46:102.
[165]. Padua, AC, Palma, S, Gruber, J, Gamboa, H, Roque, AC. Proc 11th Int Joint Conf on Biomedical Engineering Systems and Technolgies. Cliquet, A, Gamboa, H, Fred, A, Bermudez i Badia, S, editors. Vol. 1. SciTePress; Funchal, Madeira, Portugal: 2018. 48–55. BIODEVICES
[166]. Herzer N, Guneysu H, Davies DJD, Yildirim D, Vaccaro AR, Broer DJ, Bastiaansen CWM, Schenning APHJ. J Am Chem Soc. 2012; 134:7608. [PubMed: 22519954]
[167]. Manna U, Zayas-Gonzalez YM, Carlton RJ, Caruso F, Abbott NL, Lynn DM. Angew Chem, Int Ed Engl. 2013; 52:14011. [PubMed: 24288229]
[168]. Agarwal A, Huang E, Palecek S, Abbott NL. Adv Mater. 2008; 20:4804.
[169]. Platypus Technologies. [accessed: September 2019] https://www.platypustech.com/dosimeters
[170]. Wang X, Lv J, Han SEB, Zhang Y. Phys Status Solidi B. 2019; 256
[171]. Song M, Seo J, Kim H, Kim Y. Sci Rep. 2017; 7

Europe PMC Funders Author Manuscripts

Europe PMC Funders Author Manuscripts

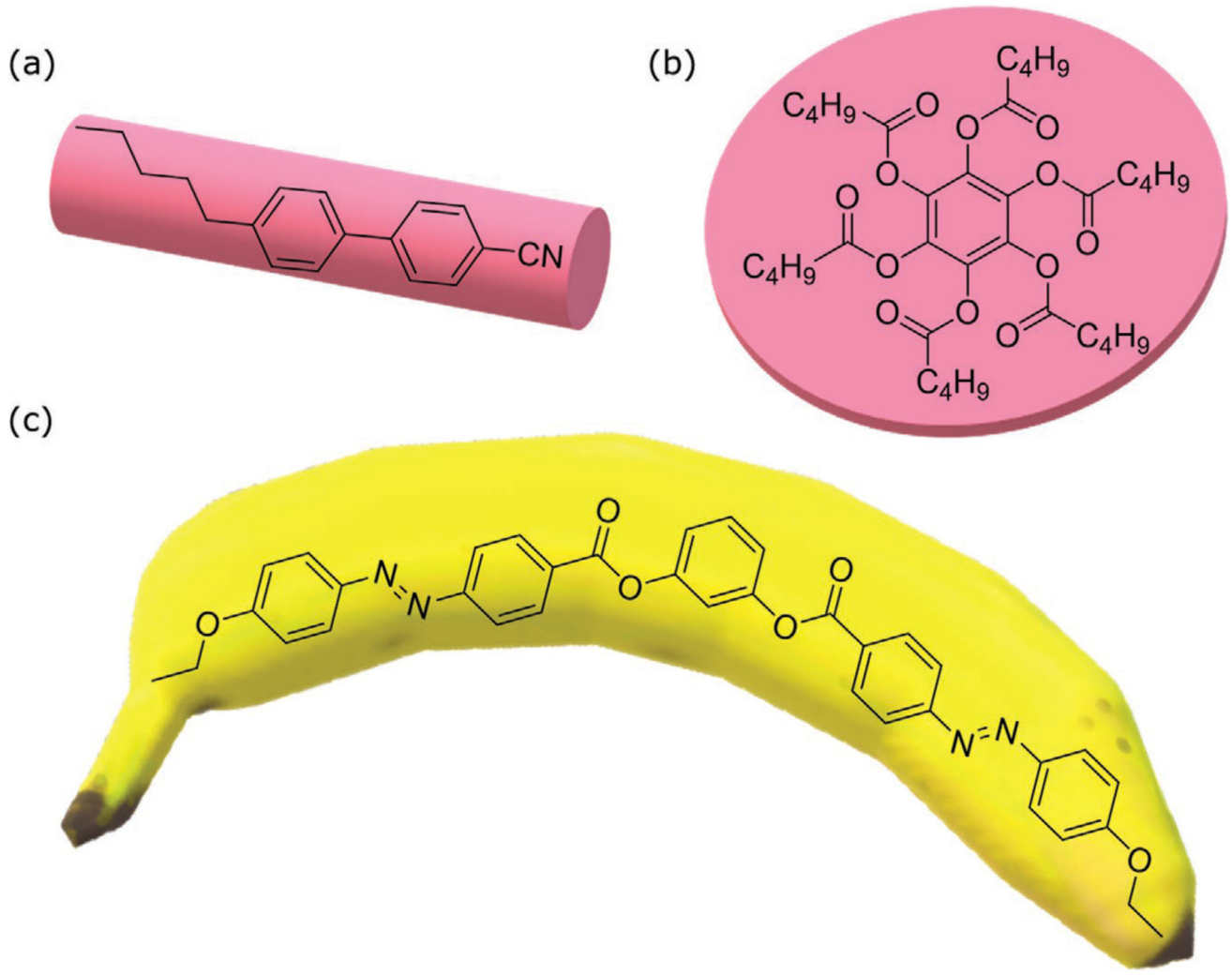

Figure 1.

Geometrical shapes of the three main building blocks forming liquid crystalline phases: a) rod shaped, 4-cyano-4′-pentylbiphenyl (5CB), b) disc shaped, benzene-hexa-n-alkanoate derivative, c) banana-shaped (or bent-core), 3:1,3-phenylene bis(4-(4-ethoxyphenyl) diazenyl) benzoate.

Europe PMC Funders Author Manuscripts

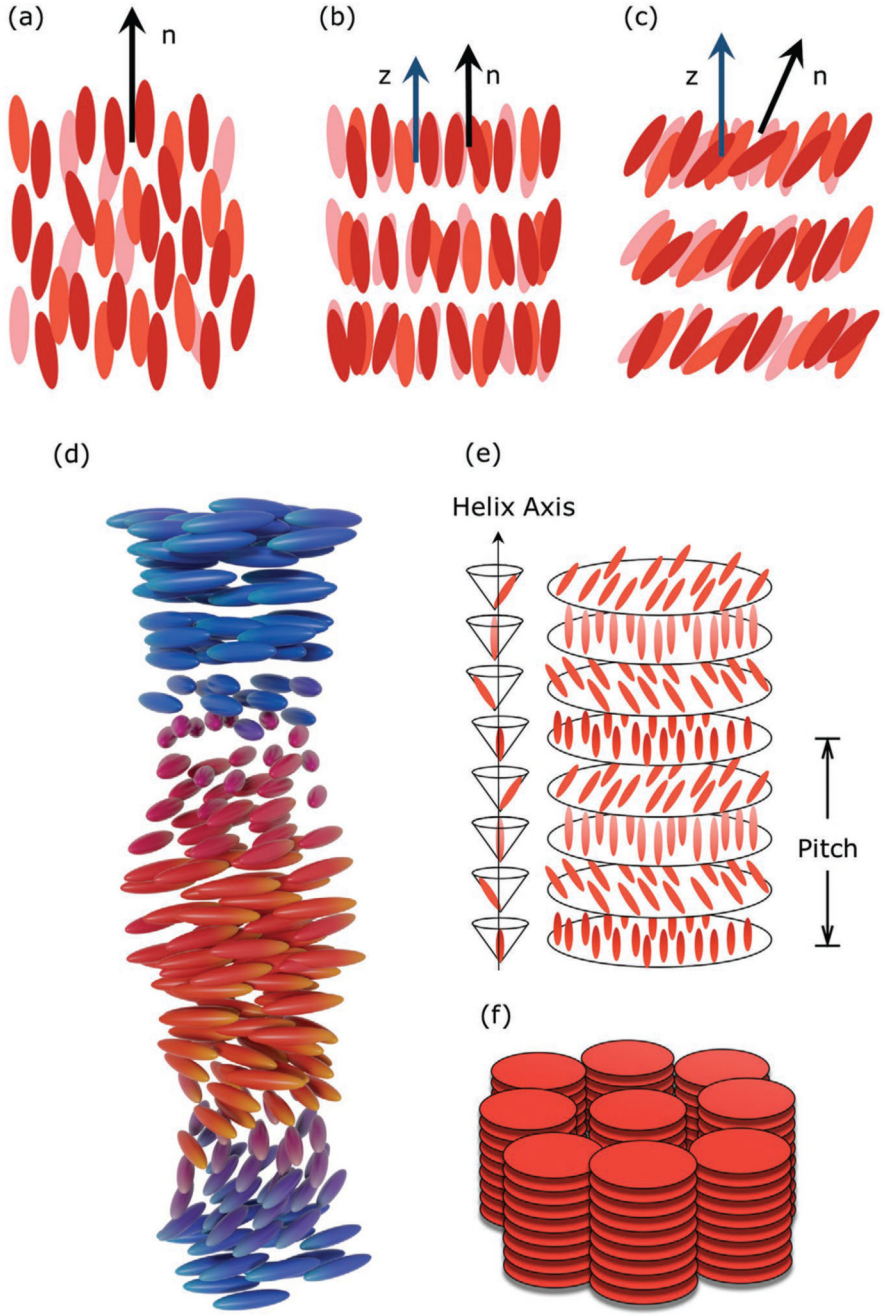

Figure 2.

Schematic arrangement of rod-shaped molecules in typical thermotropic liquid-crystalline mesophases. a) Nematic phase. The average molecular orientation is signified by the dark arrow running along the long molecular axis, namely the director $\hat{n}$. b) Smectic A phase. The director is oriented parallel to the layer normal (here the z axis represented by the blue arrow). Within the layers the molecules are isotropically distributed. c) Smectic C phase. The director is tilted with respect to the layer normal (blue arrow). Within the layers the molecules are isotropically distributed. d) Chiral nematic phase. Here, the pitch is drawn

orders of magnitude smaller than in reality. e) Chiral smectic C phase. The sketch to the left depicts in a simplistic way the chiral twist of the director along the helix axis. f) Columnar phase comprised of disc-shaped molecules stacking their cores on top of each other in a hexagonal arrangement.

Europe PMC Funders Author Manuscripts

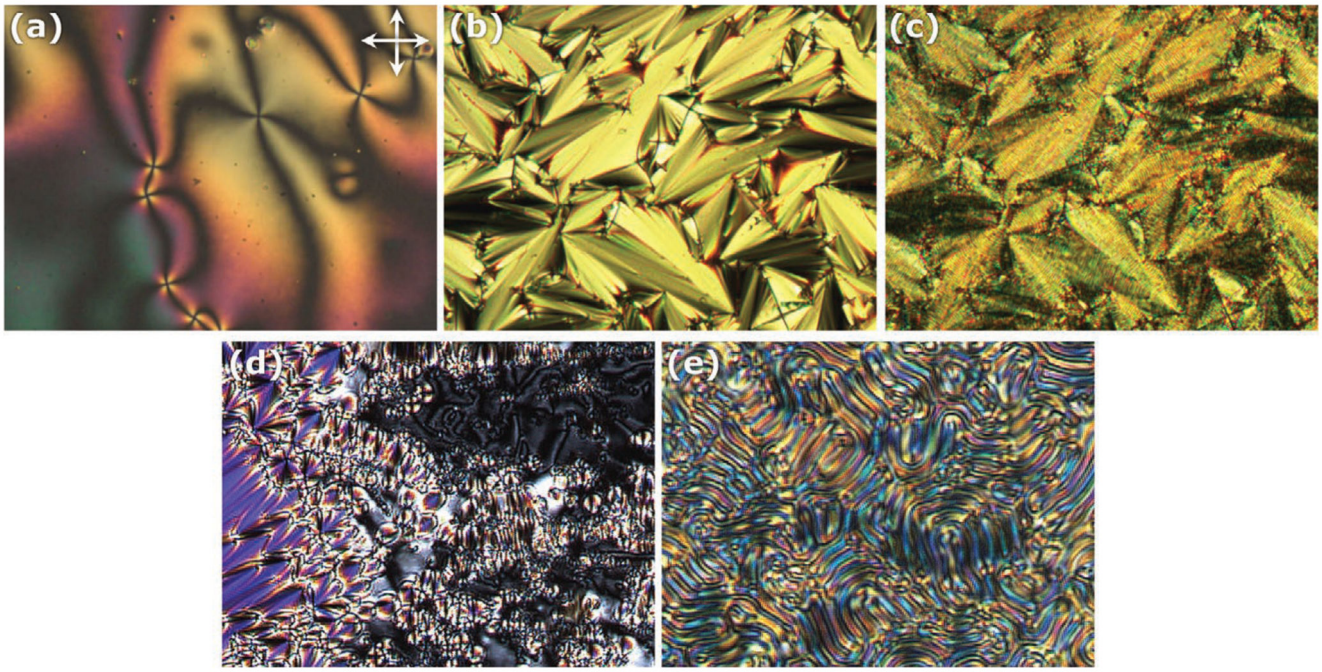

Figure 3.

Typical liquid crystalline phase textures of samples prepared on untreated glass slides observed between crossed polarizers using a polarizing optical microscope. a) Schlieren texture of the nematic phase featuring dark brushes and point defects. b) Fan-shaped pattern of smectic A phase. c) Chiral smectic C phase exhibiting a broken fan-shaped texture and line pattern that denotes the existence of a helical structure. d) Focal conic and schlieren texture of smectic C phase. e) Fingerprint texture of the chiral nematic phase. The line pattern is due to the helical structure of the mesophase.

Europe PMC Funders Author Manuscripts

Europe PMC Funders Author Manuscripts

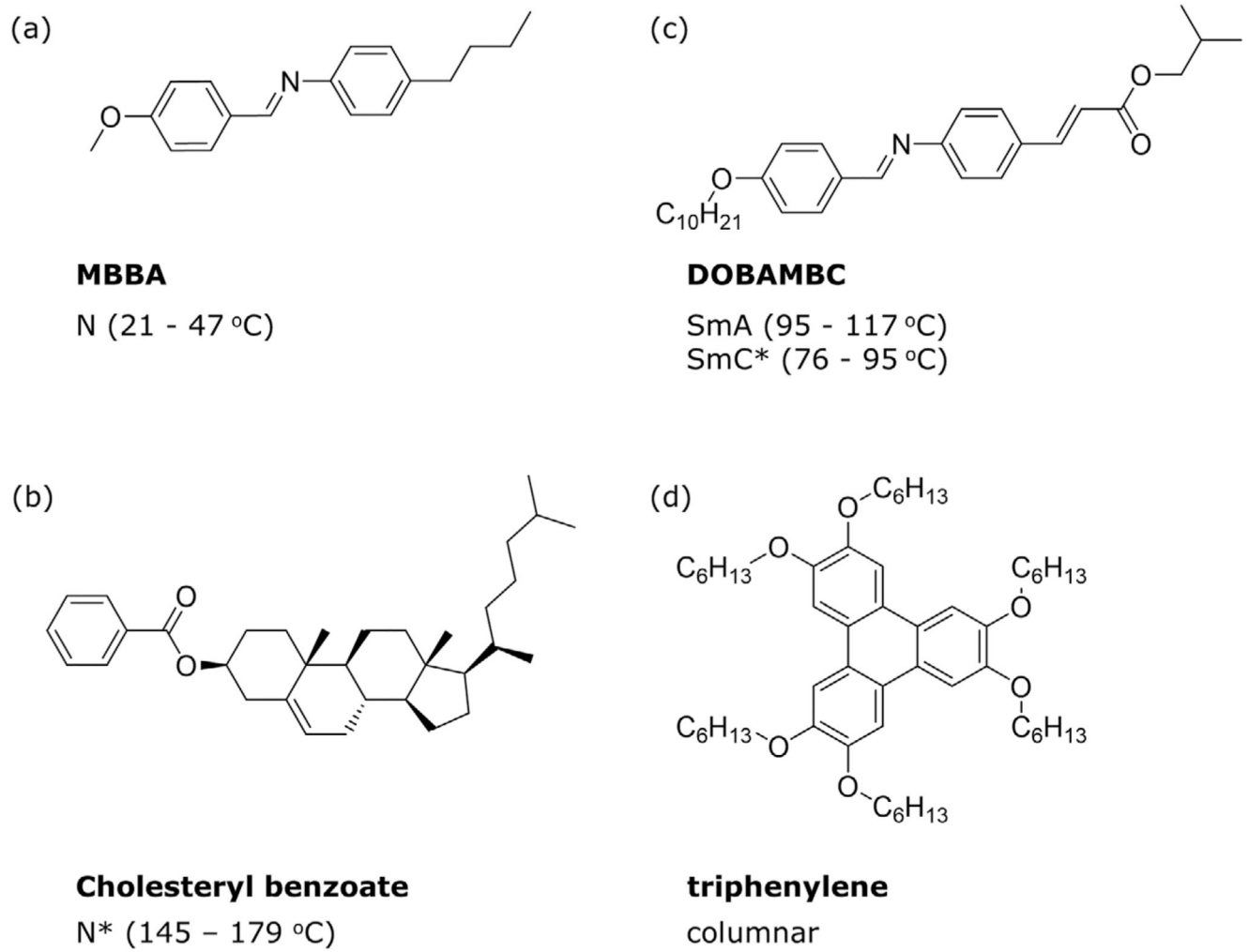

Figure 4.

Molecular structures of the most common mesogens forming liquid crystalline mesophases and corresponding transition temperatures: a) N-(p-methoxybenzylidene)-p-butylaniline (MBBA), b) 5-cholesten-3-yl benzoate (cholesteryl benzoate), c) D-2-methylbutyl 4–[4-n-decyloxybenzylideneamino]- cinnamate (DOBAMBC), d) 2,3,6,7,10,11-hexakishexyloxytriphenylene (a triphenylene derivative).

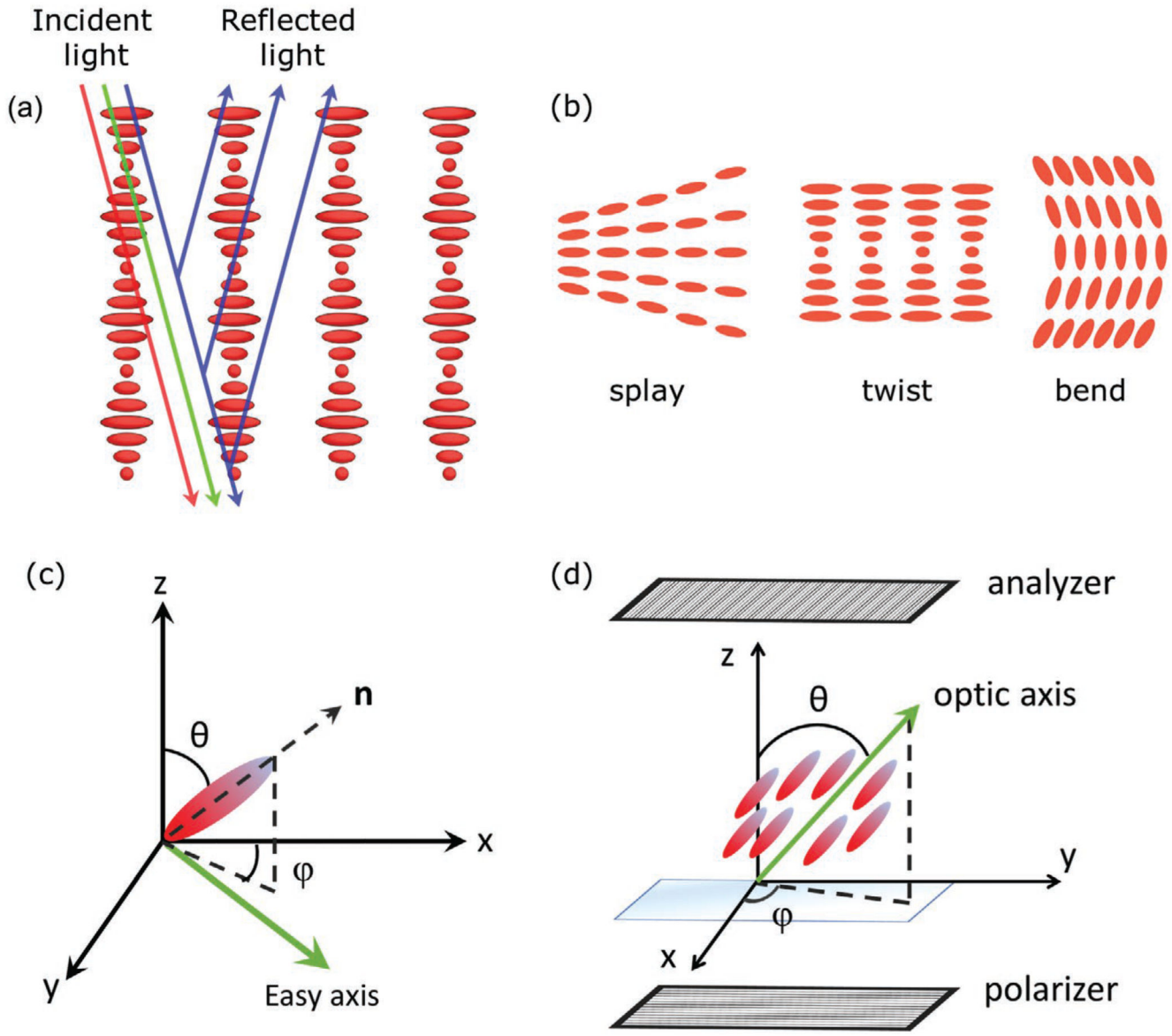

Figure 5.

Schematic representation of a) selective reflection in a chiral nematic liquid crystal. Depending on the pitch length of the helix, the refractive indices of the material and the wavelength of the light, right (left) handed structures can allow the transmission of left (right) handed circularly polarized light through the medium and reflect right (left) handed circularly polarized light. b) The three basic director deformations splay, twist, and bend. c) Definition of the zenithal (θ) and azimuthal (φ) director angles for the characterization of the preferred orientation of a liquid crystal, set by alignment (easy axis) on a flat surface. d) A well-aligned uniaxial liquid crystal between crossed polarizers for the definition of transmitted light intensity upon normal incidence.[77]

Europe PMC Funders Author Manuscripts

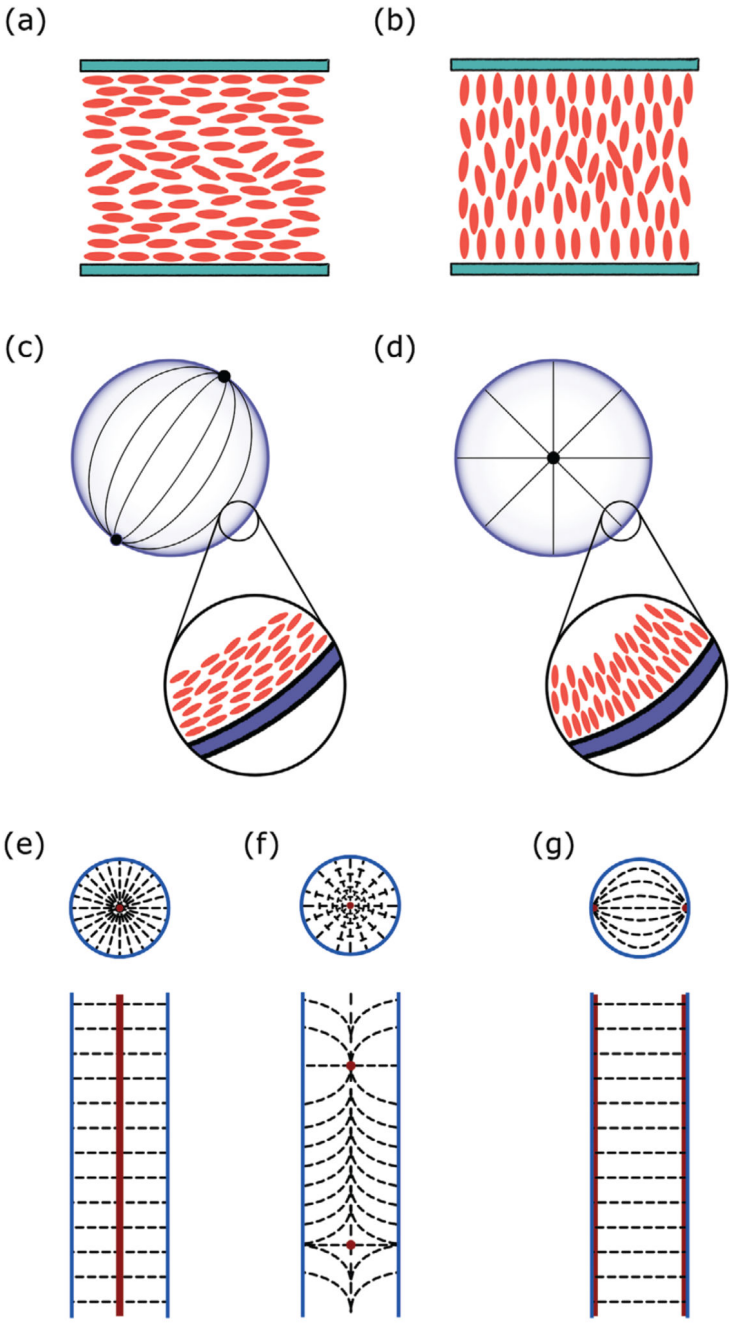

Figure 6.

Typical director configurations for the nematic mesophase on a,b) flat surfaces, c,d) spherical interfaces and e–g) cylindrical interfaces. a) Planar alignment. b) Homeotropic alignment. c) Bipolar configuration due to planar anchoring in a droplet formation. d) Radial configuration due to homeotropic anchoring in a droplet formation. c,d) The director field is schematically represented by the solid lines. The black dots depict point defects, which are characteristic of the corresponding director profile. The mesogenic molecules are denoted in the inset as red “cylinders” and the anchoring interfaces are shown in blue. e–g) The upper

drawing represents an equatorial cross-section of the cylinder and the lower drawing represents a meridional cross-section though the middle of the cylinder. e) Radial configuration with a disclination line along the core for homeotropic anchoring. f) Escaped radial with point defects for homeotropic anchoring. g) Planar bipolar configuration for planar anchoring.

Europe PMC Funders Author Manuscripts

Europe PMC Funders Author Manuscripts

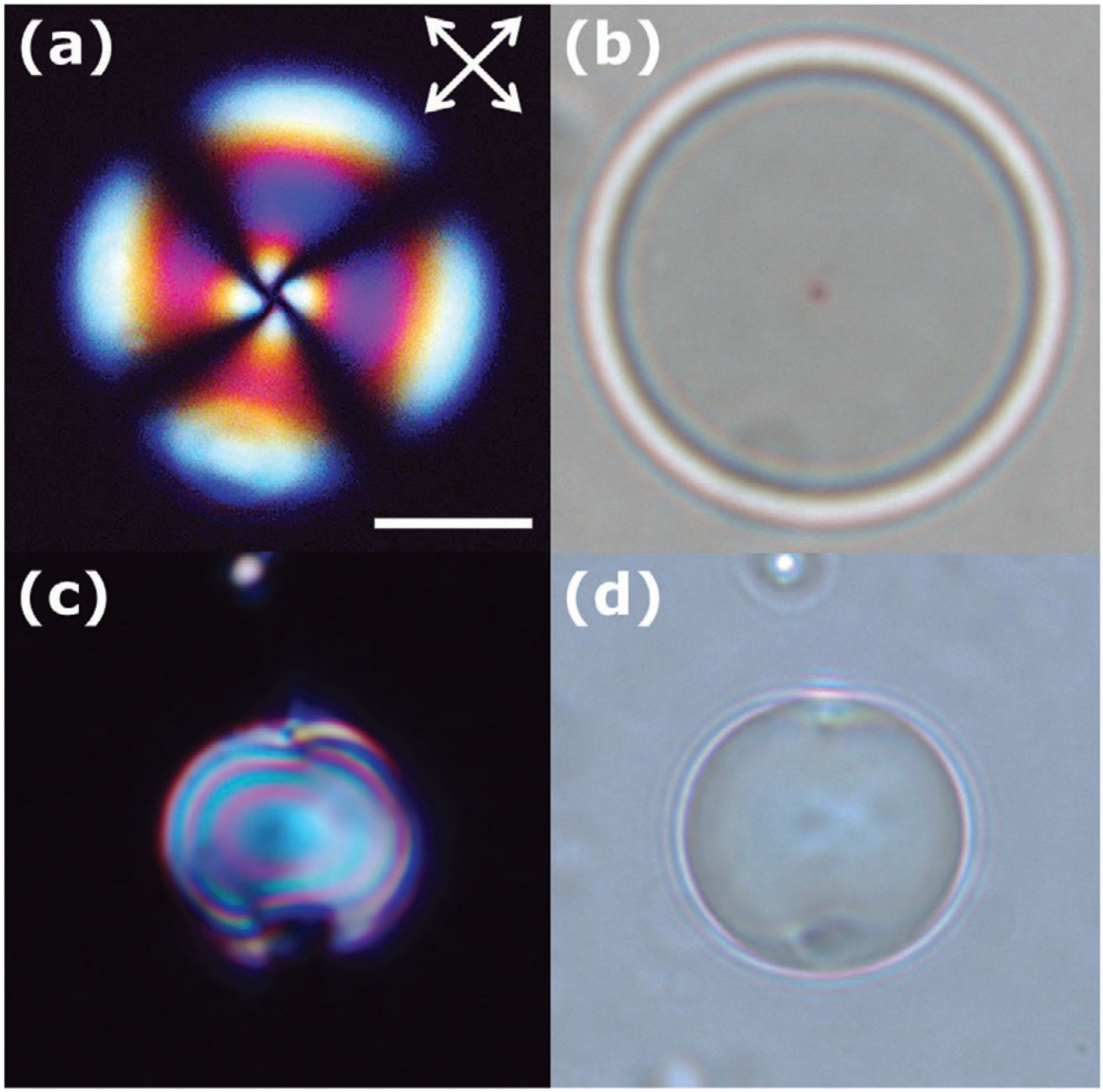

Figure 7.

a,b) Polarized light and bright-field microscopy images of nematic droplets with homeotropic anchoring. a) The extinction branches match the corresponding directions of the polarizers. b) Bright-field microscopy is used to visualize the core defect of the radial director profile named hedgehog and c,d) planar anchoring. c) The polarized light optical texture of the bipolar droplet depends on the position of the sample with respect to the crossed polarizers. d) Bright field microscopy enables the identification of the two surface defects, named boojums. The scale bar corresponds to 10 μm.

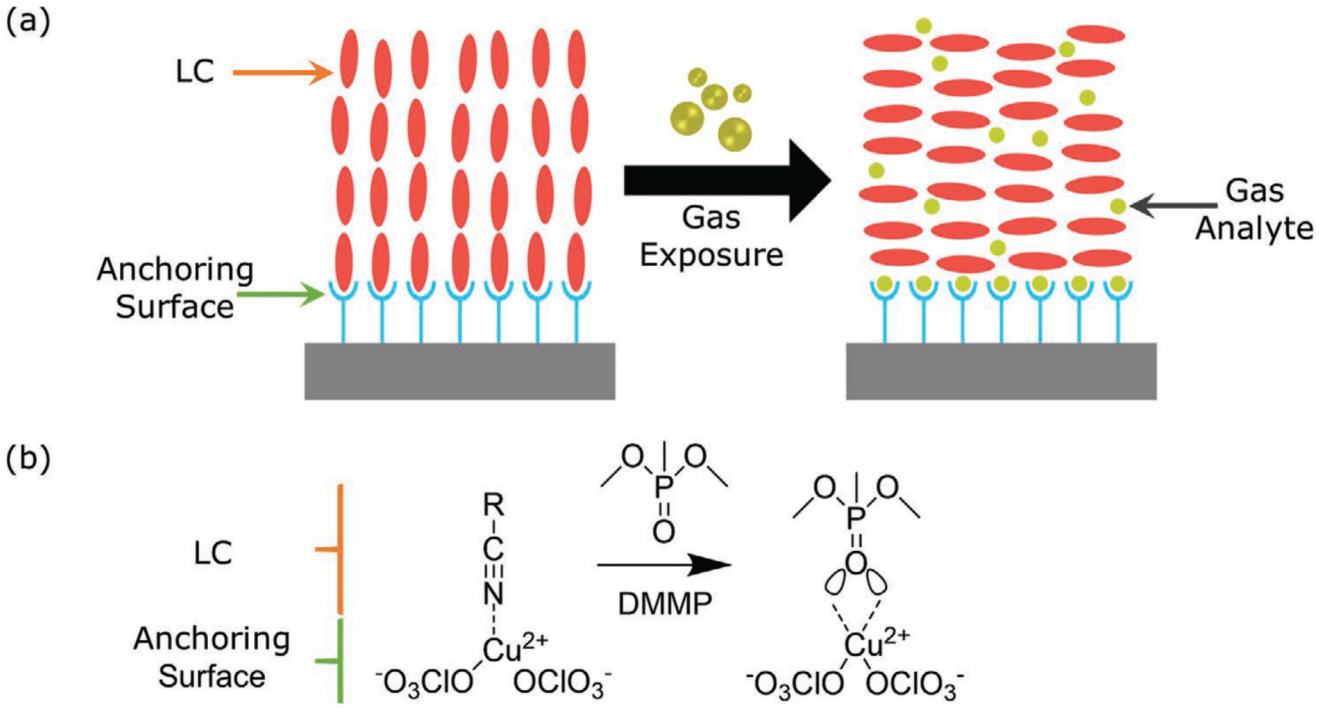

Figure 8.

Orientational transition upon gas exposure for a liquid crystal supported on a chemically functionalized surface. a) Schematic illustration of the change in molecular ordering of a homeotropically aligned liquid crystal to a planar reorientation, upon gas exposure, caused by the competition between gas and liquid crystal molecules for the binding sites on the aligning substrate. b) Molecular interactions between copper (II) perchlorate (chemically modified substrate) and the nitrile group of 5CB and the imminent disruption by the phosphoryl group of the chemical analyte DMMP (dimethyl methyl phosphonate).

Europe PMC Funders Author Manuscripts

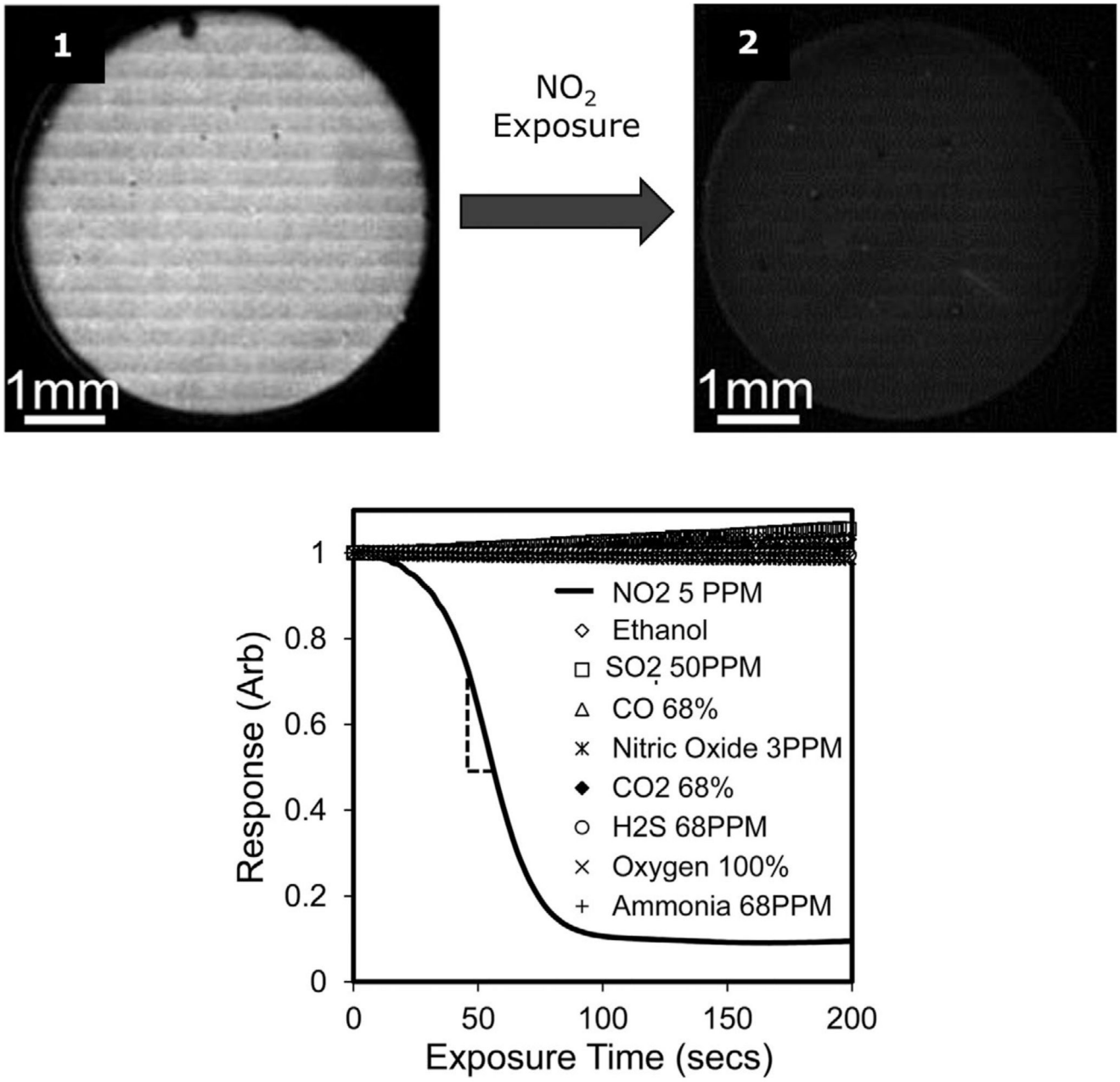

Figure 9.

Polarized optical microscopy images of a thin film of E7 supported on a gold surface, for NO_2 detection in real time. When viewed between crossed polarizers the sensor appears bright before NO_2 exposure (1) and dark when exposed to NO_2 (2), due to binding of NO_2 on the gold that leads the LC to an orientational transition. The corresponding transmitted light response shows the selectivity of the sensor towards NO_2, since it does not respond when exposed to other gases such as ammonia, ethanol etc. Adapted with permission.[46] Copyright 2013, Elsevier B.V.

Europe PMC Funders Author Manuscripts

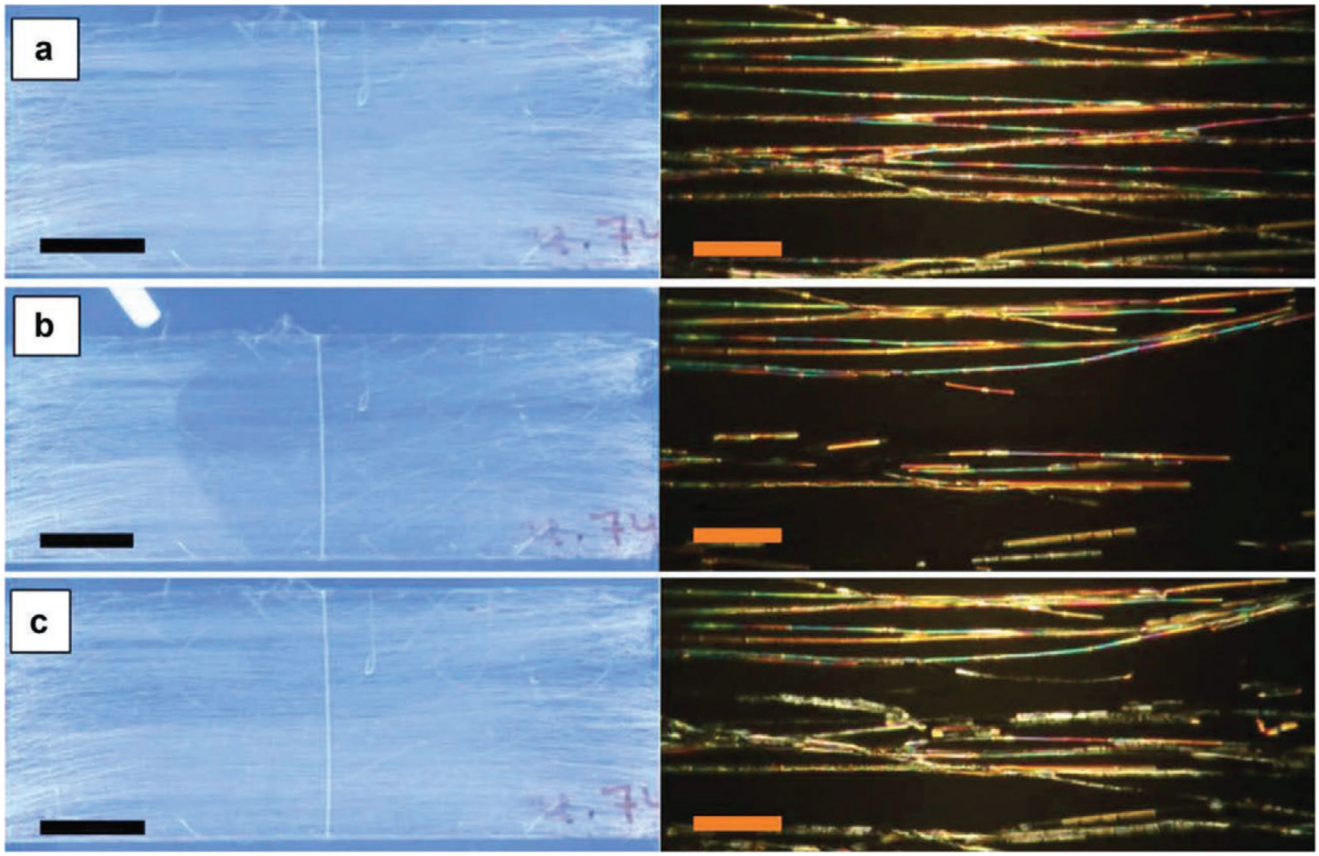

Figure 10.

Aligned mat with coaxially spun PVP-5CB fibers a) before, b) during and c) after toluene exposure. Images on the left were taken when the mat was observed under nonchromatic crossed polarizers (scale bar 10 mm). In the right column, the images were captured during POM observation of the mat using crossed polarizers (scale bar 80 μm). Reproduced with permission under the terms of the CC-BY-NC-ND 4.0 license.[44] Copyright 2016, The Authors, published by Taylor & Francis.

Europe PMC Funders Author Manuscripts

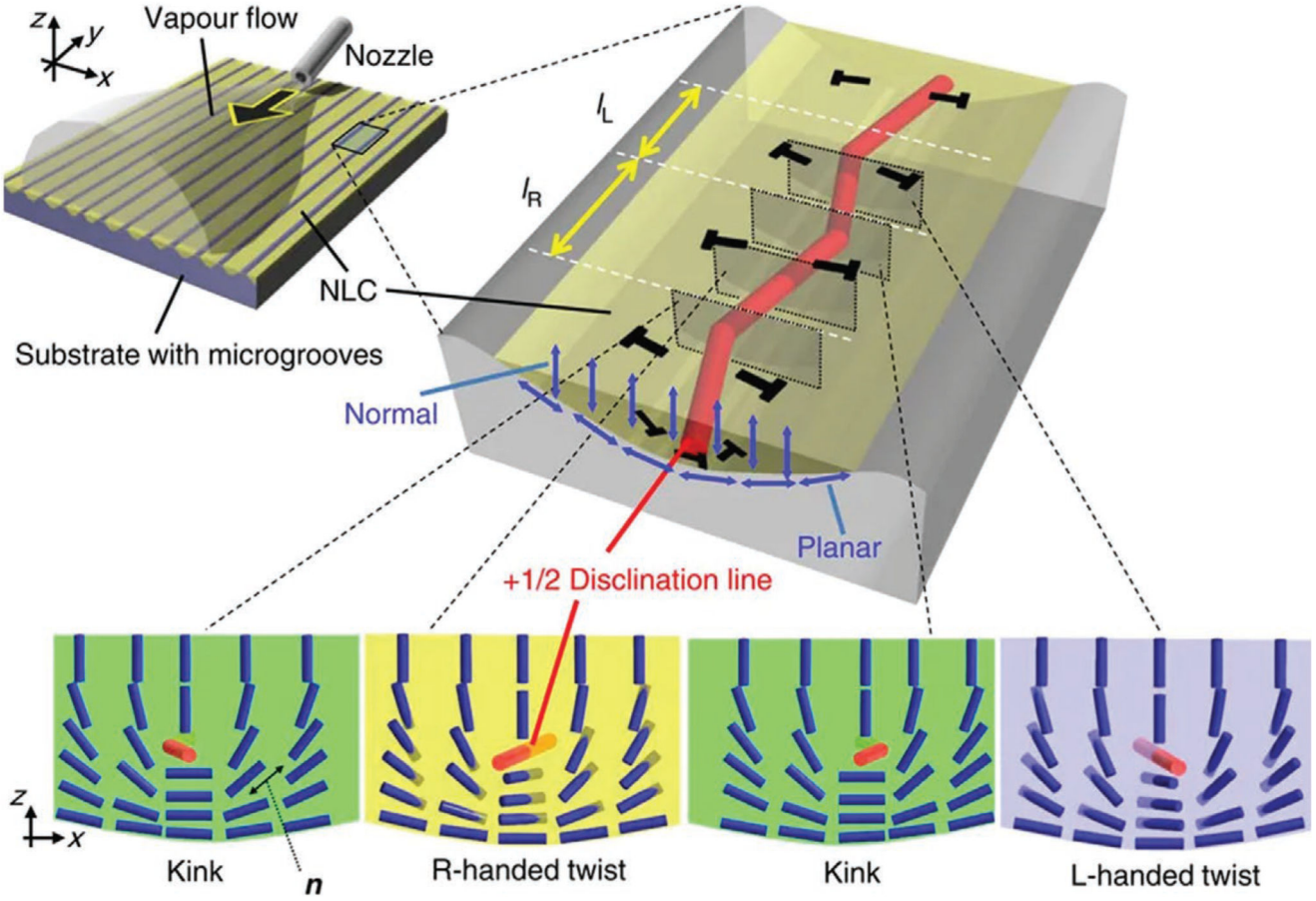

Figure 11.

Schematic representation of the experimental setup developed by Ohzono et al.[137] for chiral discrimination of vapors and director configurations within different domains along the zigzag disclination line. The gas vapor is injected through the nozzle depicted in the figure. The response can be monitored via POM. Reproduced with permission under the terms of the CC-BY-NC-ND 3.0 license.[137] Copyright 2014, The Authors, published by Springer Nature.

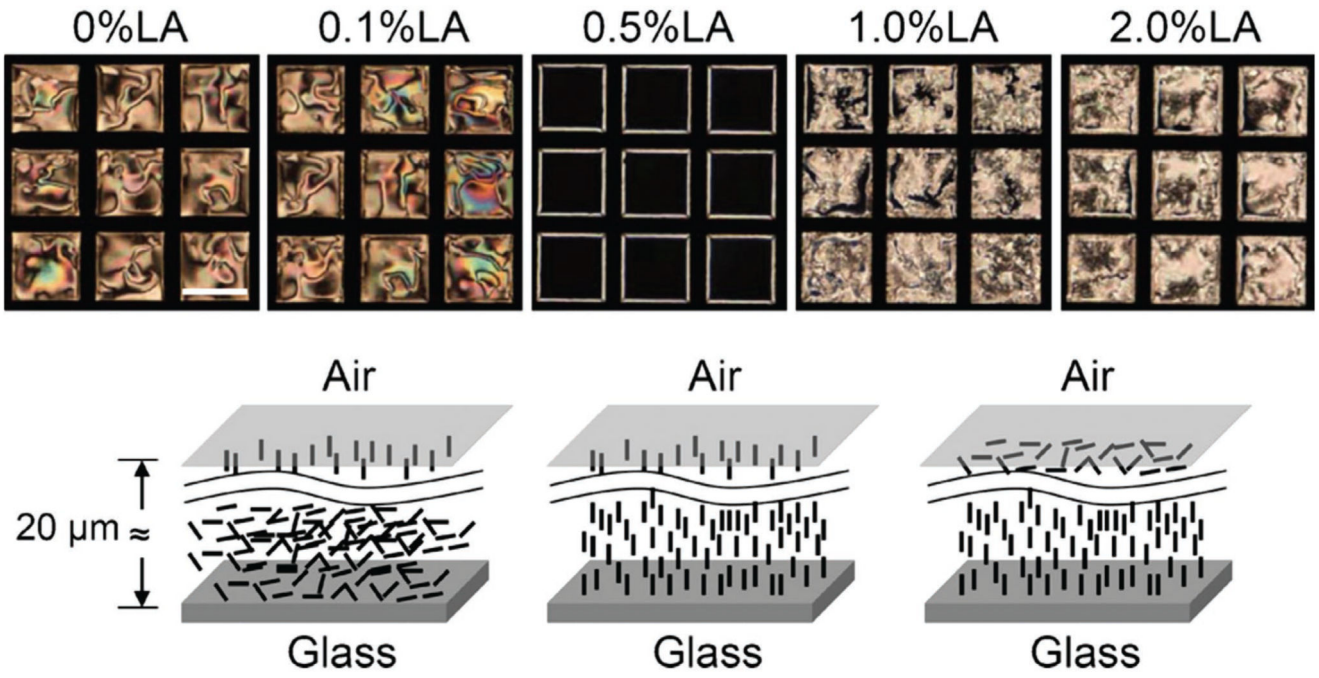

Figure 12.

Representation of the director configuration of 5CB doped with lauric aldehyde (in a range of different concentrations), and confined in copper grids, at the LC/glass and LC/air interfaces. Corresponding polarized optical microscopy images captured 2 h after sample preparation. Scale bar, 250 μm. Reproduced with permission.[139] Copyright 2012, Elsevier B.V.

Europe PMC Funders Author Manuscripts

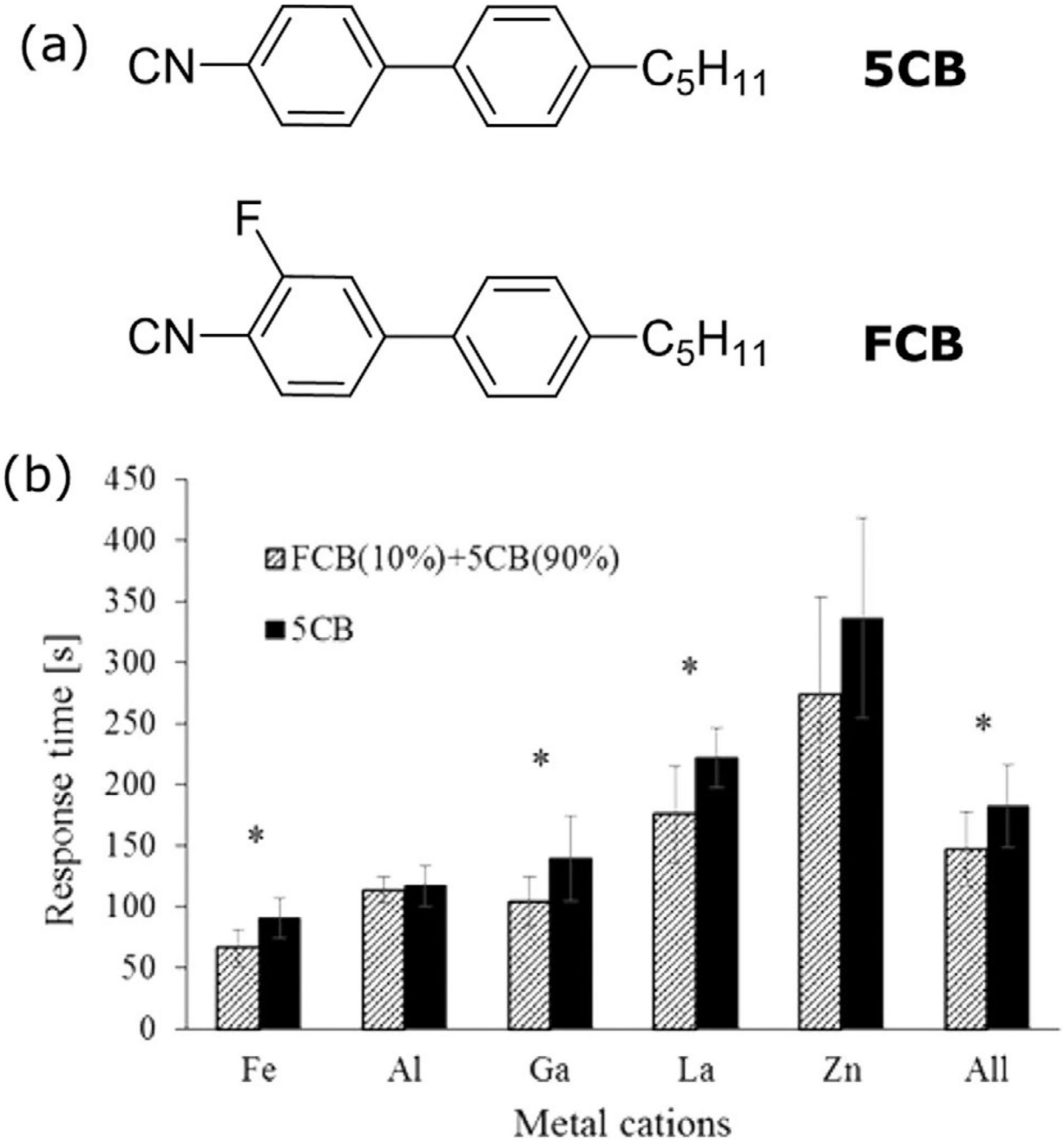

Figure 13.

a) Chemical structures of 4′-n-pentyl-4-biphenylcarbonitrile (5CB), and 3-fluoro-4′-pentyl[1,1′-biphenyl]-4-carbonitrile (FBC). b) Response times of pure 5CB and 5CB/FCB mixture (90 wt% 5CB - 10 wt% FCB) supported on surfaces coated with 10×10^{-3} M of five different metal perchlorate salts following exposure to DMMP. The last column is an average over all metal cations. Asterisks indicate a statistically significant difference in the results between 5CB and the mixture FCB/5CB. Reproduced with permission.[138] Copyright 2017, American Chemical Society.

Europe PMC Funders Author Manuscripts

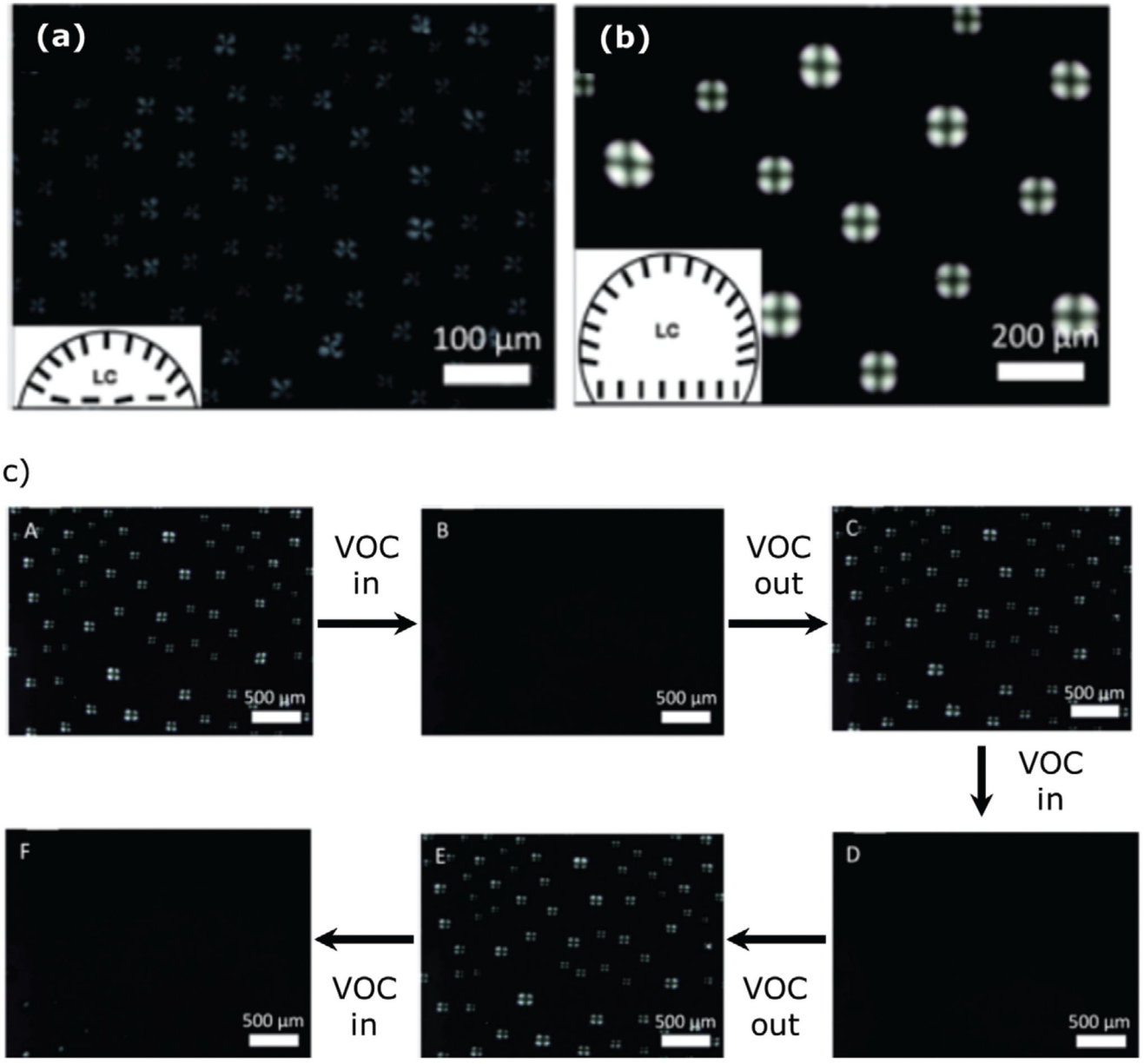

Figure 14.

Polarized optical microscopy images of liquid crystal droplet patterns formed by spreading 1 μL solution of a) ethyl alcohol containing 1% (v/v) 5CB on a piranha treated glass slide and b) heptane containing 10% (v/v) 5CB on octyltrichlorosilane (OTS) treated glass slide. c) Polarized optical microscopy images of droplet patterns on an OTS treated glass acquired in order to evaluate responses upon VOC exposure: A) in room environment, B) 5 s after incubation in heptane vapors, C) immediate exposure to the room environment, D) after a subsequent 5s incubation in heptane vapors, E) immediate exposure to the room environment again, and F) 18 s after subsequent incubation in ethyl alcohol vapors. Adapted with permission.[143] Copyright 2013, The Royal Society of Chemistry.

Europe PMC Funders Author Manuscripts

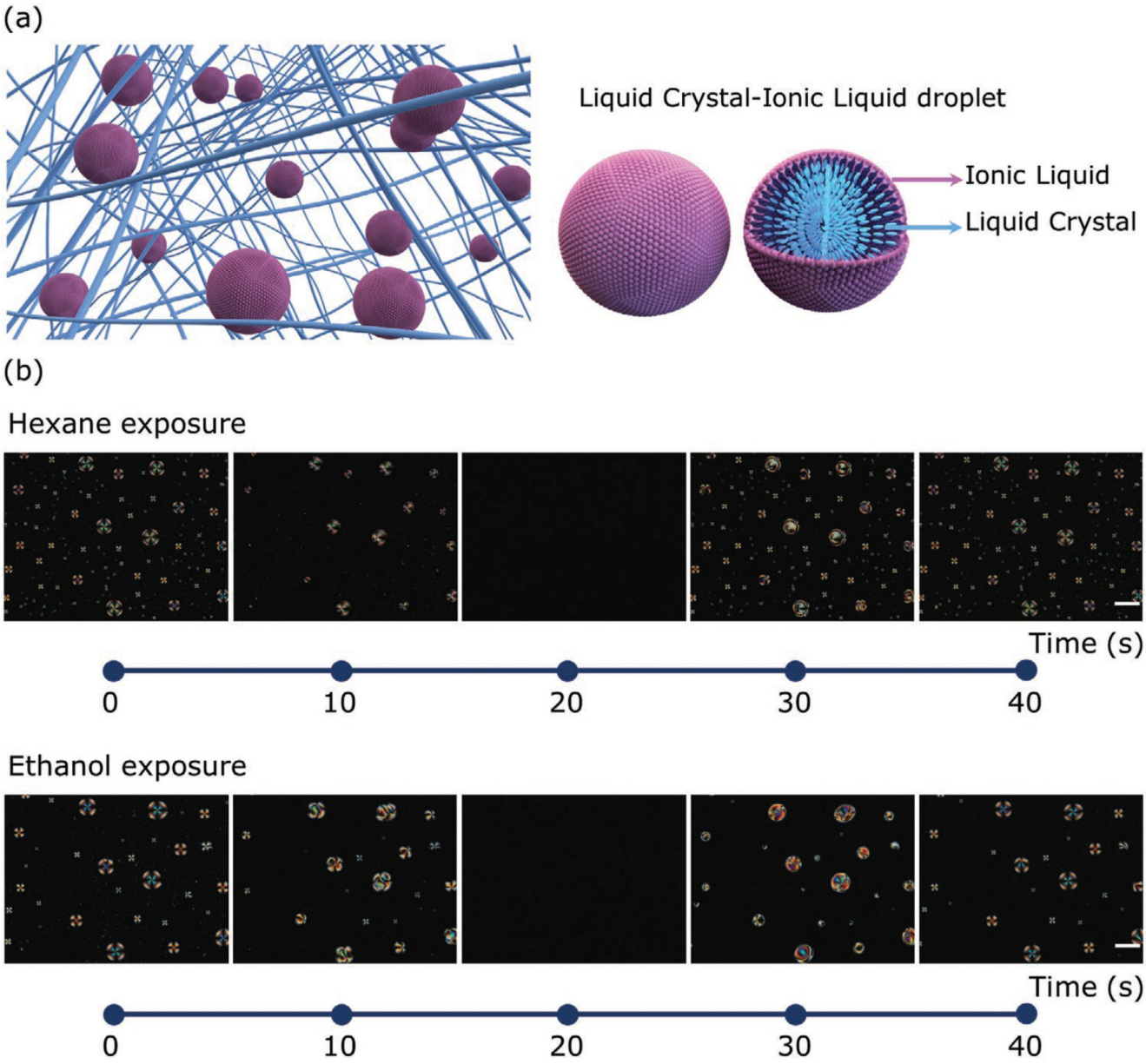

Figure 15.

Multicomponent hybrid gel films: a) schematic illustration of the compartmentalization and organization within the gels, showing the ionic liquid–liquid crystal droplets supported on the biopolymer network. b) Sequence of polarizing optical microscopy images of hybrid gel films during exposure to air saturated in hexane and ethanol. VOC injection was performed at 10 s and clean air was introduced at 25 s for hexane and 28 s for ethanol. The scale bars represent 100 μm. Reproduced with permission.[42] Copyright 2017, John Wiley and Sons.

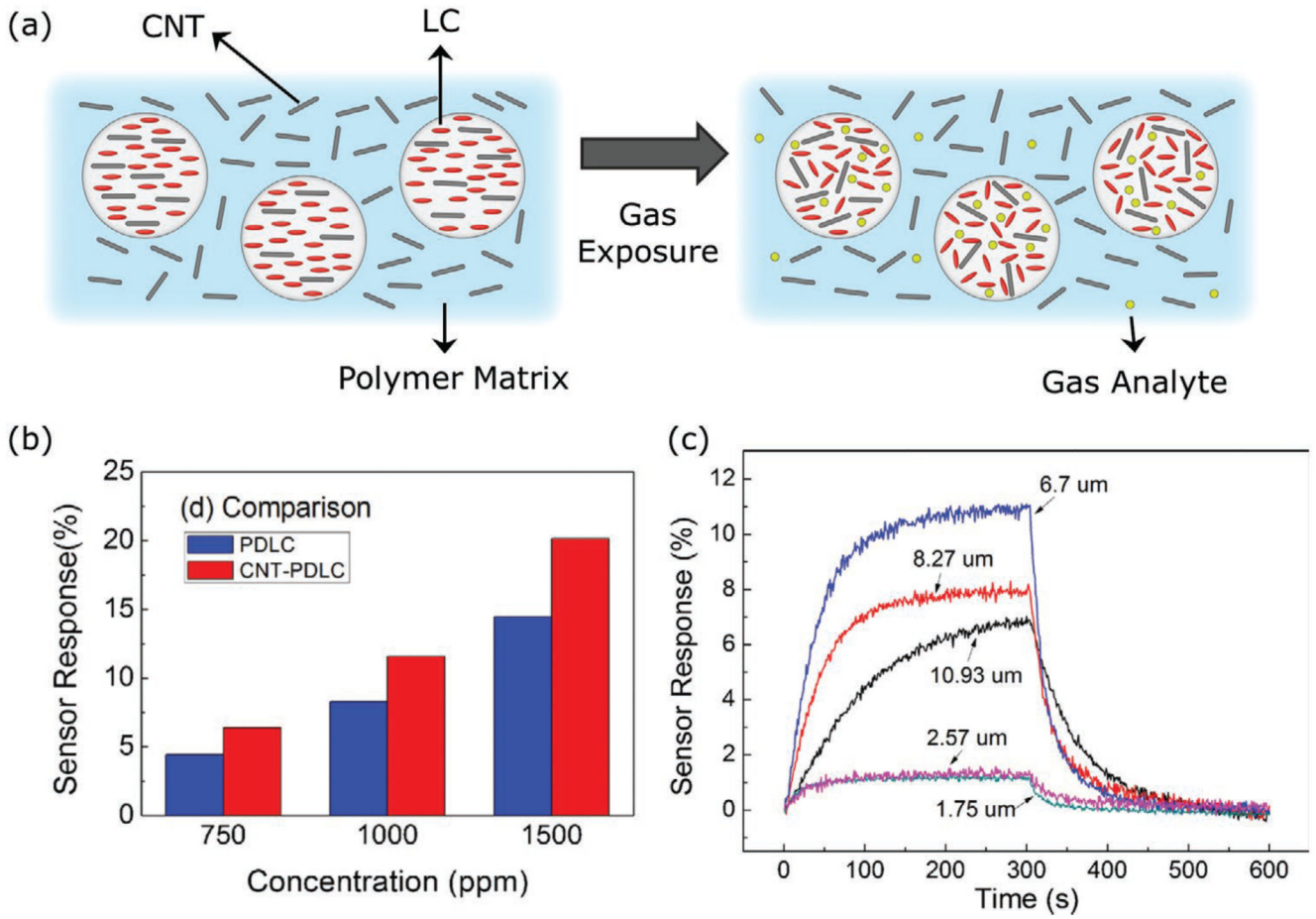

Figure 16.

Polymer-dispersed liquid-crystal sensor doped with carbon nanotubes: a) Schematic representation of the molecular ordering, before and after acetone vapor exposure. b) Comparison of the response of the pure polymer dispersed liquid crystal sensor (PDLC) and polymer dispersed liquid crystal doped with carbon nanotubes (CNT-PDLC) sensor for different concentrations of acetone. c) Influence of film thickness on the response of the CNT-PDLC sensor. Reproduced with permission.[144] Copyright 2014, Elsevier B.V.

Europe PMC Funders Author Manuscripts

Europe PMC Funders Author Manuscripts

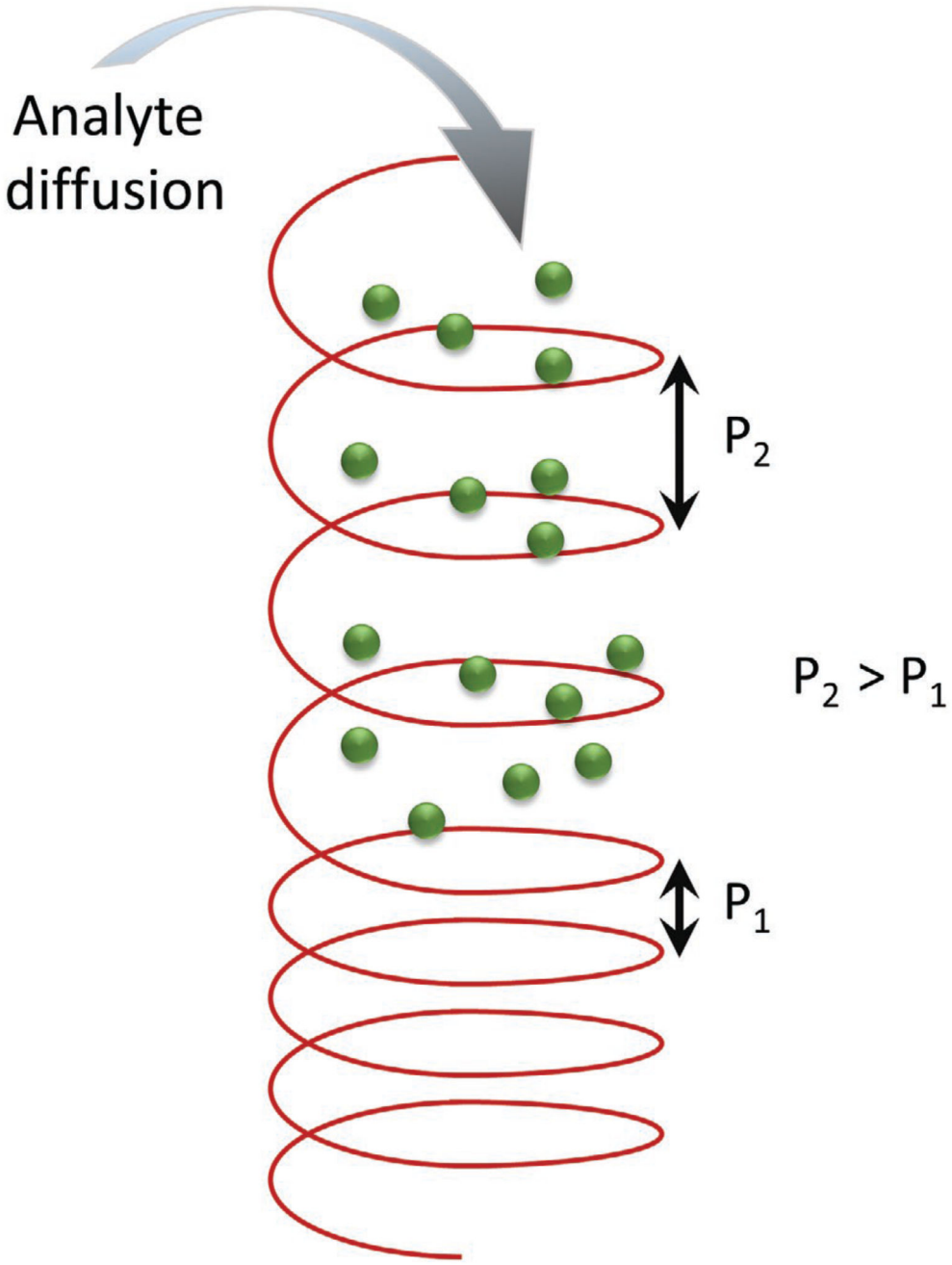

Figure 17.
Schematic representation of swelling of the chiral liquid crystal system which leads to an alteration in magnitude of the chiral pitch, upon interaction with gas molecules. Redrawn from Shibaev et al.[48]

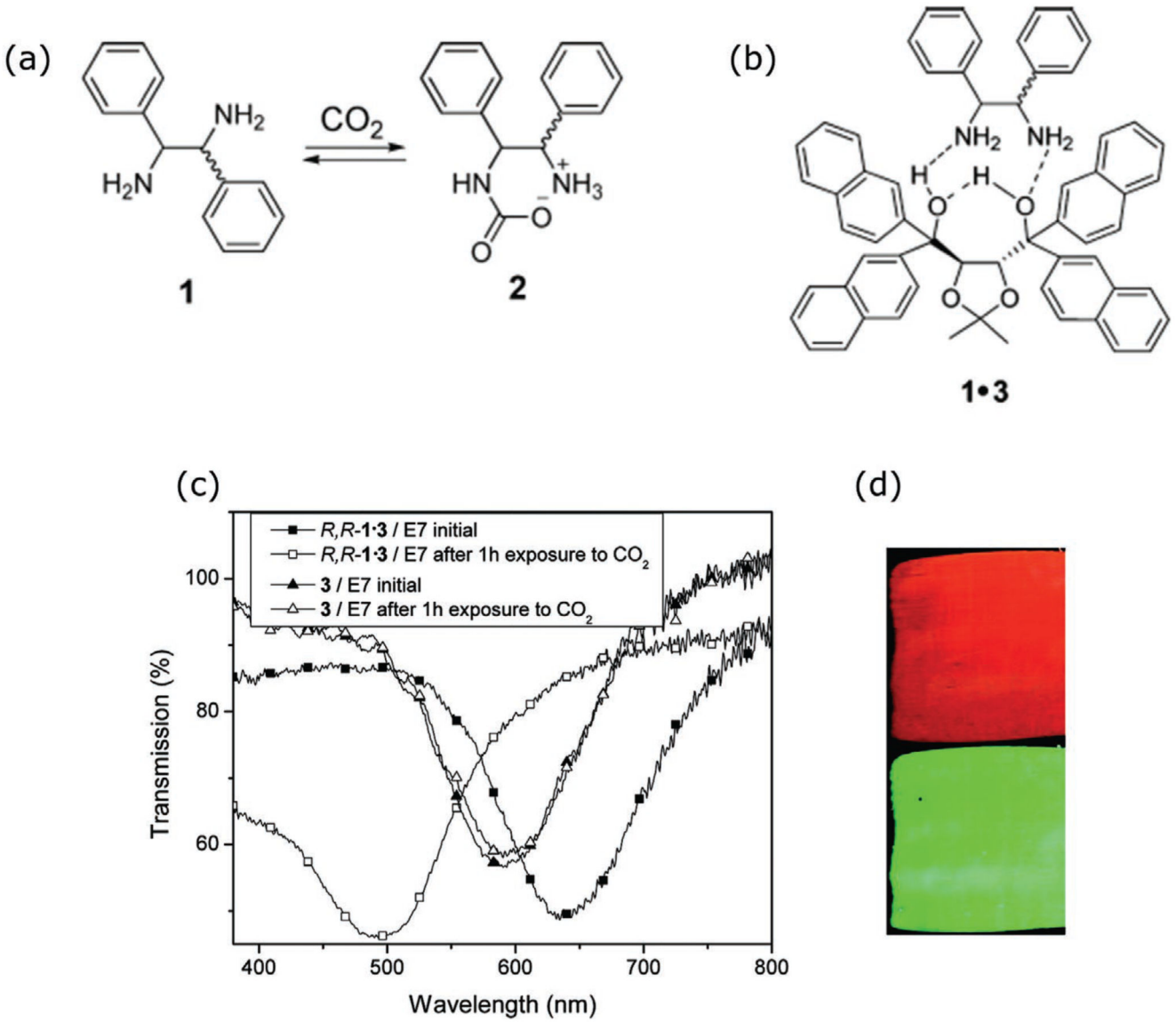

Figure 18.

a) Chiral dopant containing diamine groups (**1**) that transforms into a carbamate (**2**) upon CO_2 exposure. b) Complex chiral dopant **1.3** (produced via mixing **3**, a TADDOL derivative, with **1**) used by Han et al.[162] to dope E7 (LC host). c) Transmission spectra of E7 samples doped with **1.3** and **3**, before (closed symbols) and after (open symbols) exposure to CO_2. d) Images of an E7 sample doped with **1**, before (top) and after (bottom) exposure to CO_2 for 1h. Reproduced with permission.[162] Copyright 2010, American Chemical Society.

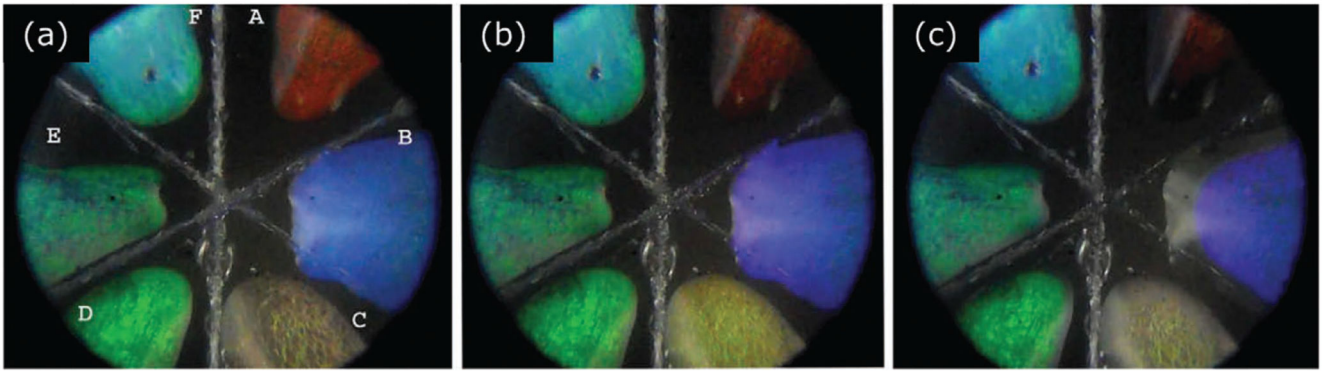

Figure 19.

Color changes of six chiral liquid crystal droplets with different compositions (from A to F) as observed with polarizing optical Microscopy. a) Initial state, b) response to 5 μL of cyclohexane, c) response to 10 μL of cyclohexane. Reproduced with permission.[48] Copyright 2019, Taylor & Francis.

Europe PMC Funders Author Manuscripts

Table 1

Liquid crystal-based gas sensing devices using solid functionalized surfaces.

	Liquid crystal	Sensing material	Detected analyte (gas or VOC)	Transduction method	Analyte interaction with sensing material	Refs.
Nematic LCs	5CB	LC film deposited onto chemically modified gold coated glass substrate with SAMs of MUA, covered with metal salts with mixed anions	DMMP	Optical (POM)	Reorientation of the LC due to the disruption of the coordination between 5CB's nitrile group and the metal ion, due to the presence of the VOC	[129]
	5CB	LC film deposited onto gold coated glass substrate chemically modified with MUA and aluminum perchlorate	DMMP	Optical (POM)	Reorientation of the LC due to the disruption of the coordination between 5CB's nitrile group and the metal ion (Al^{3+}), due to the presence of the VOC	[117,118]
	5CB	LC thin film supported on a micropillar array *a)* modified with copper perchlorate	DMMP	Optical (POM)	Reorientation of the LC due to the disruption of the coordination between 5CB's nitrile group and the metal ion (Cu^{2+}), due to the presence of the VOC	[107,108]
	5CB	LC film assembled on top of microgroove patterned amino-terminated organic substrate chemically modified with copper perchlorate salts	DMMP	Optical (POM)	Reorientation of the LC due to the disruption of the coordination between 5CB's nitrile group and the metal ion (Cu^{2+}), due to the presence of the VOC	[114]
	5CB	LC layer supported on a thiol-sensitive layer containing metal ions	Thiol vapors	Optical (POM)	Reorientation of the LC tuned by thiol-Cu^{2+} affinity	[116]
	5CB	LC thin film supported on a micropillar array *b)* modified with copper perchlorate	DMMP	Optical (POM)	Reorientation of the LC due to the disruption of the coordination between 5CB's nitrile group and the metal ion (Cu^{2+}), due to the presence of the VOC	[120]
	5CB	Thin layer of LC on an AEAPS functionalized DMOAP-coated glass slide	Glutaraldehyde	Optical (POM)	Reorientation of the LC due to the reaction between glutaraldehyde and AEAPS	[124]
	5CB	LC film deposited onto chemically modified gold coated glass substrate with SAMs of MUA, covered with different metal perchlorate salts	DMMP	Optical (POM)	Reorientation of the LC tuned by competitive binding of 5CB and DMMP to the cations of the metal salts	[126]
	5CB	LC film between gold substrates modified with mixed SAMs containing –COOH functionalities	n-Hexylamine	Optical (POM)	Reorientation of the LC anchored at the surface through interaction with –COOH due to competitive binding of NH_2 from the VOC	[130,131]
	5CB	LC film between gold substrates modified with mixed SAMs containing –COOH functionalities (1.) or deposited on chemically modified gold surfaces treated	Hexylamine (1.) DMMP (2.)	Optical (POM)	Reorientation of the LC anchored at the surfaces tuned by competitive binding of the VOC analytes to –COOH (1.) and Cu^{2+} (2.)	[115]

	Liquid crystal	Sensing material	Detected analyte (gas or VOC)	Transduction method	Analyte interaction with sensing material	Refs.
		with copper perchlorate (2.)				
	5CB	LC film on top of chemically modified glass substrate with chitosan–copper perchlorate	Ammonia	Optical (POM)	Reorientation of the LC due to the disruption of the coordination between 5CB's nitrile group and the metal ion (Cu^{2+}), due to the presence of the VOC	[113]
	5CB	LC film on glass substrates cover with manganese perchlorate	Chlorine gas	Optical (POM)	Reorientation of the LC due to the disruption of the coordination between 5CB's nitrile group and the metal ion due to the oxidation of Mn^{2+} salts to Mn^{4+} in the presence of chlorine and water vapor	[128]
	5CB	LC thin film between glass substrates covered with metal salts	DMMP	Optical (POM)	Reorientation of the LC due to the disruption of the coordination between 5CB's nitrile group and the metal ion, due to the presence of the VOC	[45]
	5CB	LC film on the bottom of polymeric wells modified with aluminum perchlorate	DMMP water	Optical (POM)	Reorientation of the LC due to the disruption of the coordination between 5CB's nitrile group and the metal ion (Al^{3+}), due to the presence of the VOC	[121]
	5CB	LC film on the bottom of polymeric wells modified with metal perchlorates	DMMP water	Optical (POM)	Reorientation of the LC due to the disruption of the coordination between 5CB's nitrile group and the metal ion, due to the presence of the VOC	[122]
	E7	LC film deposited on gold coated glass surface with polymer micropillars modified with lead perchlorate; top glass surface modified with OTS	Hydrogen sulfide	Optical (POM)	Reorientation of the LC due to the disruption of the coordination between 5CB's nitrile group and the metal ion (Pb^{2+}), due to the presence of the VOC	[127]
	E7	LC film deposited on gold coated glass surface with polymer micropillars modified with aluminum perchlorate	DMMP	Optical (POM)	Reorientation of the LC due to the disruption of the coordination between 5CB's nitrile group and the metal ion (Al^{3+}), due to the presence of the VOC	[119,123]
	E7	LC film deposited on polyurethane microwells functionalized with gold, SAM of MUA and perchlorate salts of metal ions	Organophosphorous nerve agents' vapors	Optical (POM)	Reorientation of the LC due to the disruption of the coordination between 5CB's nitrile group and the metals ion (Al^{3+}), due to the presence of competing VOC	[125]
	E7	LC film supported between two glass substrates chemically functionalized with gold, a SAM of MUA and gallium perchlorate	Diazinon	Optical (POM)	Reorientation of the LC tuned by competitive binding of the LC molecules and VOC to Ga^{3+}	[102]
	PCH3:PCH5 mixture	LC mixture into fabricated microwells with bottom surfaces decorated with lanthanum perchlorate	DMMP	Optical (POM)	Reorientation of the LC mixture due to the disruption of the coordination between LC's nitrile group and the	[133]

	Liquid crystal	Sensing material	Detected analyte (gas or VOC)	Transduction method	Analyte interaction with sensing material	Refs.
					metal ion (La^{3+}), due to the presence of the VOC	
Smectic LC	8CB	LC thin films deposited on copper perchlorate chemically functionalized gold surfaces	DMMP	Optical (spectroscopy)	Reorientation of the LC due to the disruption of the coordination between 8CB's nitrile group and the metal ion (Cu^{2+}), due to the presence of the VOC	[110]
	8CB	LC thin layer on copper perchlorate-MUA chemically functionalized goldcoated glass slides	DMMP	Optical (cross polarized equipment)	Reorientation of the LC due to the disruption of the coordination between 8CB's nitrile group and the metal ion (Cu^{2+}), due to the presence of the VOC	[109]

Notes.

a) Copper perchlorate chemically functionalized gold coated nickel micropillar glass slides

b) Nickel micropillar on top of aluminum perchlorate chemically functionalized gold coated glass slides. 8CB: 4'-n-octyl-4-cyano-biphenyl; AEAPS: N-(2-aminoethyl)-3-(trimethoxysilyl)propilamine; DMOAP: (N.N-dimethyl-N-octadecyl-3-aminopropyl)trimethoxysilyl chloride; E7: Mixture of cyanobiphenyl and terphenyls; PCH3: 4-(trans-4-propylcyclohexyl) benzonitrile; PCH5: 4-(trans-4-pentylcyclohexyl)benzonitrile; SAMs: Self-assembled monolayers.

Europe PMC Funders Author Manuscripts

Table 2
Surface topography and unconventional geometry.

Liquid crystal	Sensing material	Detected analyte (gas or VOC)	Transduction method	Analyte interaction with sensing material	Refs.
PYP-606:PYP-701	LC mixture deposited on top of unidirectional rubbed polyimide on top of silver coated glass substrate	n-alkanes cyclohexane derivatives aromatic compounds	Optical (surface plasmon resonance)	Phase transition of LC in the presence of the VOC	[135]
PYP-606:PYP-701	LC mixture deposited on top of unidirectional rubbed polyimide on top of silver-coated glass substrate	m-xylene p-xylene tetrachloroethylene	Optical (interferometry and crossed polarized equipment)	Phase transition of LC in the presence of the VOC	[134]
E7	LC film deposited on gold-coated glass surface with polymer micropillars	Nitrogen dioxide	Optical (POM)	Reorientation of the LC tuned by the affinity between gold (substrate) and the VOC	[46]
5CB	Thin films of LC supported on chemically patterned microwells in glass, gold, and polystyrene substrates	Toluene	Optical (POM)	Reorientation of the LC due to a decrease in LC anchoring allowing for the relaxation of the elastically strained LC state	[47]
MBBA Cyanobiphenyl derivatives	LC droplets placed on microscope glass slides covered with polyimide layers or sodium dodecyl phosphate	Ethyl alcohol Acetone Toluene	Optical (POM)	Phase transition of the LC in the presence of the VOC	[136]
5CB and ZLI-1132	LC anchored in open microchannels with defined periodic geometry	Chiral vapors (enantiopure compounds) Natural vapor mixtures	Optical (POM)	Imbalance of the twisted helical director distortions due to VOC interaction and its enantiomeric excess	[137]
5CB	LC functionalized PVP fiber mats	Toluene	Optical (POM and naked eye)	Phase transition of LC core due to interaction with the VOC	[44]
5CB	LC functionalized PLA fiber mats	Toluene Acetone	Optical (crossed polarized equipment)	Phase transition of LC core due to interaction with the VOC	[94]

E7: Mixture of cyanobiphenyl and terphenyls; PLA: Polylactic acid.

Table 3

Gas Sensors employing doped nematic systems.

Liquid crystal	Dopant	Sensing material	Detected analyte(gas or VOC)	Transduction method	Analyte interaction with sensing material	Refs.
5CB	DBA	DBA doped LC pipetted into copper grids placed on DMOAP-coated glass slides	Hydrazine	Optical (POM)	Reorientation of the LC due to a reaction between the dopant and the VOC	[140]
5CB	DCB	LC film onto chemically modified gold coated micropillar arrays with SAMs of MUA, covered with copper perchlorate	DMMP	Optical	Reorientation of the LC due to the disruption of the coordination between mesogen's nitrile group and metal ion (Cu^{2+}), due to the presence of the VOC	[141]
5CB	FCB F1	Thin films of LC supported on chemically patterned microwells in glass substrates or between glass substrates covered with metal salts	DMMP	Optical (POM)	Reorientation of the LC due to disruption of the coordination between nitrile group and the metal ion due to the presence of the VOC	[138]
5CB	Copper perchlorate	Copper perchlorate doped LC placed on top of BCB core and epoxy substrate	Ethanol	Optical (custom device)	Reorientation of the LC due to the disruption of the coordination between 5CB's nitrile group and the doped metal ion (Cu^{2+}) due to the presence of the VOC and increase of LC's refractive index.	[112]
5CB	Lauric aldehyde	Lauric aldehyde doped LC pipetted into copper grid placed on a clean glass slide	Octylamine Butylamine DIPA	Optical (POM)	Reorientation of the LC due to a reaction between the dopant (lauric aldehyde) and the VOCs	[139]
5CB	Copper perchlorate	Copper perchlorate doped LC pipetted into copper grid placed on glass slides	DMMP DIMP	Optical (POM)	Reorientation of the LC due to the disruption of the coordination between 5CB's nitrile group and the doped metal ion (Cu^{2+}) due to the presence of the VOC	[111]

BCB: Benzocyclobutene; DBA: 4-decyloxy benzaldehyde; DCB: 4-pentyl-3′,4′-dicyanobiphenyl; DIMP: Diisopropyl methylphoshonate; DIPA: Diisoproylamine; DMOAP: (N.N-dimethyl-N-octadecyl-3-aminopropyl)trimethoxysilyl chloride; F1: 4-Fluoro-4′-pentyl-1,1′-biphenyl.

Table 4
Gas sensing systems using nematic droplet configurations.

Liquid crystal(system)	Sensing material	Detected analyte(gas or VOC)	Transduction method	Analyte interaction with sensing material	Refs.
5CB	LC droplets: biopolymeric ionogel thin film on an untreated glass slide	Organic vapors	Optical (e-nose)	Phase transition or reorientation of the LC due to interaction with the VOC	[43]
5CB	LC droplets: biopolymeric ionogel thin film spin coated on an untreated glass slide	Tilapia fish deterioration vapors	Optical (crossed polarized equipment)	Phase transition or reorientation of the LC due to interaction with the VOC	[142]
5CB	LC droplets: biopolymeric ionogel thin film on an untreated glass slide	Organic vapors	Optical (crossed polarized equipment) and electrical	Phase transition or reorientation of the LC due to interaction with the VOC (optical signal) and changes in the system's conductance due to interaction with the matrix (electrical signal)	[42]
5CB	LC droplets deposited onto glass slides treated with piranha solution (hydrophilic) or OTS (hydrophobic)	Water Heptane Ethyl alcohol	Optical (POM)	Reorientation of the LC within the LC droplets anchored at the glass surfaces, upon VOC exposure	[143]
E7 (+CNT)	CNT–PDLC thin film on gold electrodes patterned on a silicon substrate	DMMP	Electrical	LC orientational transition, leading to restructure of CNT networks, upon VOC exposure	[145]
E7 (+CNT)	CNT–PDLC thin film on gold electrodes patterned on a silicon substrate	Acetone	Electrical	LC orientational transition, leading to restructure of CNT networks, upon VOC exposure	[144]

E7: Mixture of cyanobiphenyl and terphenyls; PDLC: Polymer dispersed liquid crystal.

Table 5

Chiral liquid crystal systems.

Liquid crystal	Dopant	Sensing material	Detected analyte (gas or VOC)	Transduction method	Analyte interaction with sensing material	Refs.
CB CN COC	–	CLCs polymer[a)] cells and thin films	Alcohol and amine vapors	Optical (spectroscopy and naked eye)	Shortening of the helical pitch due to due to formation of H-bonds between the VOC and the matrix	[146]
Licritherm TM1013	–	CLCs incorporated on a molecular imprinted polymer matrix[b)]	Methanol Ethanol Tetrahydrofuran Chloroform Tetrachloroethylene	Optical (spectroscopy) and mass (quartz crystal microbalance)	Change in the helical pitch length due to VOC absorption in the system	[153]
CN CC	–	CLC film on a glass disk with black reverse side	Acetone Benzene Hexane Pyridine	Optical (spectroscopy)	Change in the helical pitch length due to VOC absorption in the system	[147]
CC COC CN	–	CLC-coated styrene plate	Methanol Chloroform Tetrahydrofuran	Optical (spectroscopy)	Distortion of the anisotropic phase resulting in a swelling of the helical pitch due to VOC interaction with the CLC	[148]
CC CCA CN	–	CLC film coated side polished fiber	Tetrahydrofuran Acetone Methanol	Optical (spectroscopy)	Change in the helical pitch length due to VOC interaction with the CLC	[151]
E7	S1011 and DBD	CLC-coated PET films	Acetone Toluene	Optical (POM & Spectroscopy)	Change in helical pitch length and a subsequent phase transition due to VOC interaction with the CLC	[154]
E7	S1011, DBD, and CNT	CLC–CNT hybrid solution on rubbed PET films	Acetone	Optical (spectroscopy) and electrical	Change in helical pitch length and a subsequent phase transition due to VOC interaction with the system. Changes in the electrical resistance of the system	[159]

Liquid crystal	Dopant	Sensing material	Detected analyte (gas or VOC)	Transduction method	Analyte interaction with sensing material	Refs.
MBBA Cholesterol carbonate Cholesterol chloride Wacker oligomer	Cholesterol carbonate Cholesterol chloride Wacker oligomer	LC[c)] droplets on top of rubbed polyvinylalcohol-coated glass substrate	Cyclohexane Acetic acid	Optical (optical microscopy)	Phase transition of the CLCs in the presence of the VOC	[48]
Wacker oligomer	–	CLC dissolved in toluene and deposited on glass slide. Samples were heated up to 120 °C at the presence of air, pure water or solutions of polyacrylic acid	Water Ethanol Toluene	AFM	Surface pattern reconstruction	[164]
E7	Optically pure diamine-TADDOL derivative (R,R-1 and S,S-1) complex (1.) chiral binaphtyl dithiol derivative and a nonresponsive codopant – (R)-(+)-(1,1′-binaphthalene)-2,2′-dithiol (2.)	CLC thin film on planarly rubbed with a velvet cloth TAC foil or polyimide-coated glass slide	Carbon dioxide (1.) Oxygen (2.)	Optical (spectroscopy & naked eye)	Change in helical twist power of the chiral dopant due to reaction with the VOC	[162]
1,4-Di(4-(6-acryloyloxypropyloxy) benzoyloxyl)-2-methylbenzene and 4-(4-(6-acryloyloxyhexyloxy) benzoyloxy) methoxybenzene	MAA	CLC polymeric[d)] film printed on TAC foil	(1) Anhydrous TMA, (2) TMA in watersaturated nitrogen gas	Optical (spectroscopy and naked eye)	(1) Phase transition due to disruption of H-bonded polymer network upon exposure to the VOC, (2) Change in the helical pitch length due to adsorption of the VOC in the system	[149]
RM82 and RM105	LC756	Hydrogen-bridged CLC polymer networks with a porosity printed on TAC films	Alcohol vapors	Optical (spectroscopy)	Change in helical pitch length due to absorption of the VOC in the system	[155]
COC CN CB	Dodecylamine	CLCs doped with dodecylamine pasted onto clean or DMOAP-coated glass slides (reverse side black). CLC doped films covered with PDMS followed by glass slides	Aldehyde vapors	Optical (spectroscopy & naked eye)	Color change due to a reaction between the dopant (dodecylamine) and the VOC	[160]
CN COC	Oleic acid (1.) Oleyl amine (2.) Mono cholesteryl terephthaloyl chloride (3.) Cholesteryl phenyl hydrazide (4.) Cholesterol (5.) Cholesteryl chloroformate (5.) Methyl linolenate (6.)	CLC film onto thin Mylar film with black reverse side	Hydrochloric acid (1.) Hydrogen fluoride (2.) Hydrazine (3.) Unsymmetrical dimethyl hydrazine (4.) Nitrogen dioxide (5.) Nitric acid (6.)	Optical (naked eye)	Color change due to interactions with the VOC	[99]

Liquid crystal	Dopant	Sensing material	Detected analyte (gas or VOC)	Transduction method	Analyte interaction with sensing material	Refs.
E7	R,R-TADDOLphenylhydrazine complex	LC-dopant mixture spin-coated onto polyimide-coated glass slides, previously rubbed with a velvet cloth	Acetone	Optical (spectroscopy)	Change in the helical twisting power due to a reaction between the dopant and the VOC	[161]
E E1 *e)*	Magnetite NPs	LC doped with magnetite NPs absorbed into mesoporous alumina matrix	Carbon monoxide	Optical (spectroscopy)	Change in helical pitch length due to VOC interaction with dopant (magnetite NPs) and with the LC	[158]
E E1 e)	Magnetite NPs	LC doped with magnetite NPs absorbed into silicon dioxide nanocomposite	Carbon monoxide	Optical (spectroscopy)	Change in helical pitch length due to VOC interaction with dopant (magnetite NPs) and with the LC	[157]
CLC-2103L	Magnetite NPs	LC doped with magnetite NPs into optically transparent porous material	Carbon monoxide	Optical (spectroscopy)	Change in helical pitch length due to VOC interaction with dopant (magnetite NPs) and with the LC	[156]
Schiff-bases (azomethine), Demus esters, tolans (diphenylacetylene), phenylcyclohecyls, and bicyclohexanes derived LC ZLI-1083 E7 5CB	DDS-1015L & NYC-22133L	CLCs spin coated on a rubbed polyimidecoated glass substrate	Toluene Cyclohexane MEK Cyclohexane Acetone Ethanol Tert-butyl alcohol	Optical (spectroscopy)	Change in helical pitch length upon interaction of the VOC with the CLC	[152]
CN COC CC	LCR-262 *f)*	LC films on structuresupporting polymers *g)* -coated glass substrate	Amine vapors	Optical (photometry and spectroscopy)	Change in helical pitch length upon interaction of the VOC with the CLC	[150]

a) UV curable polymer Norland Optical Adhesive 61 (NOA61) and glass slide covered by another glass slide; separation distance between glasses kept by using two pieces of polyethylene spacer

b) Divinylbenzene (cross linker), styrene (monomers), AIBN (initiator) and tetrahydrofuran (solvent)

c) CLC mixtures composed of MBBA, derivatives of cholesterol and Wacker oligomer (glass-forming compound). CLC compositions → CLC-A: cholesterol carbonate (77%) and cholesterol chloride (23%); CLC-B: MBBA (59%) and CLC-C (41%); CLC-C: MBBA (80%) and Wacker oligomer (20%); CLC-D: CLC-A (90%) and Wacker oligomer (10%); CLC-E: CLC-A (80%) and Wacker oligomer (20%); CLC-F: CLC-A (65%) and Wacker oligomer (35%)

d) Other chemicals used for the CLC film: 1,4-Di(4-(6-acryloyloxypropyloxy)benzoyloxy)-2-methylbenzene (crosslinker), 4-(6-acyloyloxyhexyloxy)benzoic acid and 4-(6-acyloyloxyhexyloxy)-2-methylbenzoic acid (polymerizable benzoic acid derivative), Irgacure 369 (photoinitiator), hydroquinone monomethyl ether (thermal inhibitor) and tetrahydrofuran (solvent)

[e] Chiral LC mixture containing multiple chiral cyano-biphenyl, cyano-terphenyl derivatives, with a chiral mesophase range of 282–318 K and optical anisotropy Δn 0.234 at 589 nm, 273 K

[f] CB with a trifluoroacetyl receptor attached to a benzene moiety

[g] PMMA and EG80A (polyurethane hydrogel) and hexamethyldisilazane. CB: Cholesteryl benzoate; CC: Cholesteryl chloride; CN: Cholesteryl nonanoate; CCA: Cholesteryl carbonate; COC: Cholesteryl olelyl carbonate; CLC: Chiral liquid crystal; DMOAP: (N.N-dimethyl-N-octadecyl-3-aminopropyl)trimethoxysilyl chloride; E7: Mixture of cyanobiphenyl and terphenyls; MAA: R(+)-3-methyladipic acid; NPs: Nanoparticles; PDMS: Poly(dimethylsiloxane); PET: Polyethylene terephthalate; TAC: Triacetyl cellulose; TMA: Trimethylamine.

Europe PMC Funders Author Manuscripts